Hindawi
Advances in Materials Science and Engineering
Volume 2022, Article ID 6165180, 22 pages
https://doi.org/10.1155/2022/6165180

Research Article

Investigation of Effective Parameters Ce and Zr in the Synthesis of H-ZSM-5 and SAPO-34 on the Production of Light Olefins from Naphtha

Omer Dhia Aldeen Salah Aldeen,[1] Mustafa Z. Mahmoud,[2,3] Hasan Sh. Majdi,[4] Dhameer A. Mutlak,[5] Khusniddin Fakhriddinovich Uktamov,[6] and Ehsan kianfar [7,8]

[1]*Almaarif University College Medical Laboratory Techniques Department, Anbar, Ramadi, Iraq*
[2]*Department of Radiology and Medical Imaging, College of Applied Medical Sciences, Prince Sattam Bin Abdulaziz University, Al-Kharj 11942, Saudi Arabia*
[3]*Faculty of Health, University of Canberra, Canberra, Australian Capital Territory, Australia*
[4]*Department of Chemical Engineering and Petroleum Industries, Al-Mustaqbal University College, Babylon 51001, Iraq*
[5]*Al-Nisour University College, Baghdad, Iraq*
[6]*Economic Security Department, Tashkent State University of Economics, Tashkent, Uzbekistan*
[7]*Department of Chemical Engineering, Arak Branch, Islamic Azad University, Arak, Iran*
[8]*Young Researchers and Elite Club, Gachsaran Branch, Islamic Azad University, Gachsaran, Iran*

Correspondence should be addressed to Ehsan kianfar; e-kianfar94@iau-arak.ac.ir

Received 23 December 2021; Revised 17 January 2022; Accepted 2 February 2022; Published 24 February 2022

Academic Editor: Zhongchang Wang

In this paper, Ce and Zr modified commercial SAPO-34 and H-ZSM-5 catalysts were synthesized via a wet impregnation method and used as catalysts for the production of light olefins from naphtha. The synthesized catalysts were characterized using SEM, TGA, XRD, BET, and NH_3-TPD. Thermal catalytic cracking of parent catalysts (SAPO-34 and H-ZSM-5) and modified catalysts with Ce and Zr on the production of light olefins from naphtha has been studied. The effects of different loading of Ce (2–8 wt.%), Zr (2–5 wt.%), and different temperatures on the yield of ethylene and propylene were also investigated. The yield of ethylene and propylene improved by 21.78 wt% and 23.8 wt%, respectively, over 2% Ce and 2% Zr on SAPO-34 catalyst. This is due to the higher acid sites on the surface of modified catalysts. It was found that H-ZSM-5 with 2% Zr loading has the highest yield of light olefins (40.4%) at 650°C in comparison with unmodified parent catalysts, while Ce loading has less effect on the olefin yield compared to Zr loading. Finally, simultaneous loading of Ce and Zr showed no effect on the light olefin yield owing to the significant decline of acid sites.

1. Introduction

Light olefins, such as ethylene and propylene, are important raw materials for synthesizing many organic compounds in the industry in a huge volume including plastics, synthetic fibers, and rubber. Common technologies for these materials production are thermal catalytic cracking and fluidized bed catalyst (FCC) using ZSM-5 zeolite catalysts [1–3]. Ethylene is widely used in the plastics industry to produce polyethylene, polyvinyl chloride (PVC), polyester, etc. Ethylene and propylene are among the major petrochemical base products that have benefited over other petrochemical raw materials such as gas and naphtha. In recent years, manufacturers have an increasing attention towards the development of ethylene production versus propylene production, especially methods of producing propylene [4–8]. The thermal catalytic cracking process of naphtha hydrocarbons has been a major source of olefin production for more than half a century [9, 10] and the production of olefins varies between 24 and 55 wt. % for ethylene depending on feed type and operating conditions

and between 1.5 and 18 wt. % for propylene [11]. Despite the good progress made on this process, it still has the highest energy consumption in the petrochemical industry [12, 13]. This process requires a high temperature between 800 and 880°C, which comprises approximately 40% of the petrochemical fuel consumed, resulting in a large amount of CO_2 emissions [14, 15]. Many studies have been carried out to reduce (1) the fuel consumption and (2) CO_2 emissions during this steam cracking process, and some improvements have contributed to the literature; however, there is still lack of control over the propylene to ethylene ratio. This ratio changes with the feed type, but the demand has grown more for propylene than ethylene, so a catalytic cracking process has been proposed [16–20]. Thermal catalytic cracking process produces a large amount of ethylene along with other smaller molecules. During this process, the feed is preheated in an oven to 510–600°C, and the feed temperature should be shortened to prevent unnecessary chemical reaction during the preheating process. The heated feed is then transferred to a reactor, and the large molecules at high pressure break down into a small molecule. The catalytic cracking has been implemented to increase the production of light olefins, and it has been extensively investigated for various hydrocarbons on different types of catalysts. The process is carried out at temperatures of 550 to 650°C to produce ethylene and propylene [21–26]. The selectivity of light olefins depends on types of feed as well as catalysts, acid strength, and acid types such as Lewis and Brønsted acid sites. Catalytic cracking is a flexible process used also to break down less high molecular weight oils to produce more valuable light products. A wide range of solid acid catalysts have been used in this process. Among them, aluminum silicate is a good example of catalyst used in catalytic fluidized bed cracking (FCC), and it has a three-dimensional crystalline structure with regular cavities of molecular size [27–33]. Zeolite catalysts such as ZSM-5 and SAPO-34 have been widely used in the oil refining, petrochemical, and pollution control industries [29, 34–43]. This is because these materials have a specific porous structure and high specific surface area. Aluminum phosphate molecular sieves (ALPO) were first reported in 1982. These materials have similar structure to zeolites, but their main structure is made of Al-O-P bonds instead of Si-O-Al or Si-O-Si. Since the molecular structures of ALPO are neutral, they are not selective in catalytic process [44–54]. Therefore, the addition of silicon to the ALPO structure resulted in the formation of silicoaluminophosphate (SAPO) molecules. The addition of Si^{+4} with P^{+5} results in the formation of Bronsted acid sites, which makes these molecules more selective as catalyst for specific reaction [55–67]. Among the various SAPOs, SAPO-34 has a good selectivity to ethylene and propylene.

Cerium and lanthanum catalysts supported on SAPO-34 were employed in thermal catalytic cracking of naphtha to produce light olefins. SAPO-34 modified with Mg and Ni showed higher selectivity to light olefins and extended lifetime in the conversion of methanol to olefin. Stability of HZSM-5 modified with P and Fe was improved in naphtha catalytic cracking.

Zirconium with high mechanical strength and appropriate thermal resistance could improve the thermal stability of catalysts and prevent the sintering of the active particles. It has been reported that the addition of zirconium to cerium oxide can significantly increase reducibility, activity, and thermal stability of cerium oxide, resulting in increased resistance to coke formation. However, the low surface area of cerium and zirconium oxides is their major limitation. Therefore, the use of cerium and zirconium oxides supported on SAPO-34 could improve the performance of SAPO-34 [68–77].

In this study, we investigate the impact of Ce and Zr modified H-ZSM-5 and SAPO-34 catalysts on the production of light olefins from naphtha. The chemical structure, morphology, surface area, surface acidity, and structure stability for the catalyst are studied using X-ray diffraction (XRD), scanning electron microscopy (SEM), N_2 adsorption-desorption isotherms, ammonia probe-temperature programmed desorption (NH_3-TPD), and thermogravimetric analysis. The catalyst activities during the cracking of naphtha are tested using a pilot thermal catalytic cracking.

2. Experimental

2.1. Materials. SAPO-34 and H-ZSM-5 catalysts were purchased from ZEOCHEM, Switzerland, and the specifications of these catalysts are given in Table 1. Cerium (III) nitrate hexahydrate [$Ce(NO_3)_3.6H_2O$, 99.99% purity] and zirconium (IV) oxynitrate hydrate [$ZrO(NO_3)_3$. H_2O, 99.99% purity] were obtained from Sigma-Aldrich, while the naphtha fraction was provided from Iran and used without further purifications.

2.2. Synthesis of Catalysts. Cerium and zirconium with specific weight ratios were impregnated into SAPO-34 and H-ZSM-5 catalysts using wet impregnation method. A certain amount of $[Ce(NO_3)_3.6H_2O$ and $ZrO(NO_3)_3$. H_2O was added into a round-bottomed flask containing dispersed catalyst in 25 ml of distilled water and gently stirred for 2 h at room temperature. The resulting suspension was refluxed at 75°C in a water bath for 1 h. The obtained solution was then oven-dried at 120°C for 2 h, prior to calcination in furnace under static air at 750°C for 1 h in order to get rid of any remaining impurities. The obtained catalysts were sieved in the range of 10–20 mesh size [78–81].

2.3. Catalyst Characterizations. Wide-angle powder X-ray diffraction (XRD) was carried out on a Bruker D8 diffractometer or Philips with Cu Kα ($\lambda = 1.5418$ Å) radiation and a LynxEye detector between 5 and 80° with steps of 0.035° at 10 s per step. The particle size, morphology, and surface structure of catalysts were determined using a Hitachi operated at 15 kV. Texture properties were measured by the multipoint nitrogen adsorption-desorption method at 77 K on a Micromeritics TriStar 3000 porosimeter or NOVA-2000 Quantachrome porosimeter. Catalyst samples were degassed in vacuo overnight at xx °C prior to analysis. The temperature programmed desorption (TPD) ammonia (NH_3) was

Table 1: Texture properties and compositions of SAPO-34 and H-ZSM-5 catalysts.

Catalysts	BET surface area (m^2/gr)	Pore volume (cm^3/g)	Crystallite size (μm)	Si/Al
SAPO-34	573	0.28	7	0.24
HZSM-5	443	0.26	4	50

performed on a Micromeritics Auto Chem II analyzer coupled with a thermal conductivity detector (TCD). The catalyst sample was heated from room temperature to 800°C under a constant flow rate of helium purge gas at 30 ml/min before carrying out the measurement. The catalyst sample was firstly cooled down to 100°C and then followed by conducting ammonia adsorption for 1/2 h using an ammonia flow rate of 30 ml/min. After saturation with ammonia, the catalyst was purged with helium at 30 ml/min for 1.5 h to eliminate any unreacted ammonia before the measurement. The temperature ramped from 100 to 800°C at 10°C/min under helium purge gas of 30 ml/min and then held at 800°C for 1/2 h. The desorbed species from catalyst sample monitored by TCD and the density of acid sites was quantified. Thermogravimetric analysis (TGA) was performed on a Mettler Toledo (TGA/DSC-1) by programming the system to heat up from room temperature (25°C) to 900°C at 20°C/min under a constant flow rate of nitrogen gas at 50 ml/min.

2.4. Thermal Catalytic Cracking Reactor Setup. The thermal catalytic cracking pilot plant unit is illustrated in Figure 1. The raw material feed and water were injected into a stirred stainless steel reactor for mixing, and the resulting solution was then mixed with the steam before feeding into the preheating unit at xx. The mixture was heated to 500°C in a furnace. The obtained gases from the thermal catalytic cracking were quenched by passing through a series of condensers. The released gases were analyzed by online GC-MS (Agilent 6890 N chromatograph-560S mass spectrometer) according to the reported methods [35–37, 71–75].

The physical properties and chemical composition of naphtha feed are presented in Table 2.

2.5. Operational Conditions for Thermal Catalytic Cracking. In the case of SAPO-34 catalyst, all experiments were considered at 750°C, 1.2 g/min of naphtha inlet mass flow rate and SR = 0.5 and performed over 1 g of SAPO-34 catalyst with 4 g silicon carbide. The summary of operating conditions is given in Table 3. Sic was used as an inert to increase the amount of catalyst substrate inside the reactor. The main reason for choosing SiC was because it has low density, low thermal expansion, high strength, high thermal conductivity, and high heat shock resistance and can, therefore, be an excellent neutralizer for the thermal catalytic cracking reaction [82–86].

However, in the case of H-ZSM-5 catalyst, all experiments were considered at 750°C, 2 g/min of naphtha inlet mass flow rate and SR = 0.5 and performed over 1 g of H-ZSM-5 catalyst with 4 g SiC. The summary of operating conditions is presented in Table 4 [85–87].

3. Results and Discussion

3.1. XRD Analysis of Catalyst SAPO-34. Figure 2 shows the XRD results of Ce-modified SAPO-34 catalysts. Also, shown in Figure 3 are the results of XRD analysis for Zr -modified SAPO-34 catalysts, and the XRD catalysts modified by the synergy of Ce and Zr are also shown in Figure 4. Generally, in all catalysts, the peak intensities decrease with the addition of unmodified catalysts due to the presence of amorphous catalysts, which can be attributed to the presence of amorphous materials such as Ce and Zr. According to Figures 2–4, the position of the peaks has not changed at different loading rates. According to the XRD images, all the catalysts have a chabazite structure, and their structure has not changed significantly after correction. According to Figure 2 with increasing cerium, the intensity of SAPO-34 peaks decreased, and cerium peaks appeared. According to Figure 2, with increasing cerium, new cerium peaks appeared at $2\theta = 28.54, 33.08, 47.49$, which is consistent with the results of Jiangnan et al. As shown in Figure 3, the crystallinity of SAPO-34 decreased with increasing Zr, but no Zr peak appeared. This is due to the diffusion of Zr particles onto the surface of the catalyst at the nanoscale [87–89].

3.2. XRD Analysis of Catalyst HZSM-5. The effect of adding different amounts of Ce and Zr on HZSM-5 is investigated in Figures 5 and 6. As can be seen by adding different amounts of Ce and Zr, the position of the zeolite peaks has not changed, indicating that the basic catalyst crystal structure is maintained after salt addition. New peaks have been added to the base catalyst, indicating the presence of metals. In Figure 5, the addition of Ce metal on the base catalyst is investigated. The apparent peak intensities for Ce are short, indicating that the metal is well dispersed on the base. The intensity of Ce metal peaks increased with increasing loading percentage. The effect of Zr metal loading on the base catalyst is investigated in Figure 6. The pigment intensity of Zr is very low, indicating that the metal is well dispersed on the surface, and the dispersed Zr dimensions are less than 3 nm. The addition of Ce metal to the catalyst with 2% Zr in Figure 7 and the addition of Zr metal to the catalyst with 2% Ce in Figure 8 are shown. Maintaining the basic structure, increasing the intensity of the peaks with increasing loading rates, and decreasing the peak intensities of these two metals are the results obtained from these shapes. The increase in peak intensity can be observed in the XRD analysis of the modified HZSM-5 catalyst with 8% Zr. This increase in crystallinity can be attributed to the removal of aluminum out of the xenolith structure due to the reaction with Zr. This results in a more regular base catalyst structure [90, 91].

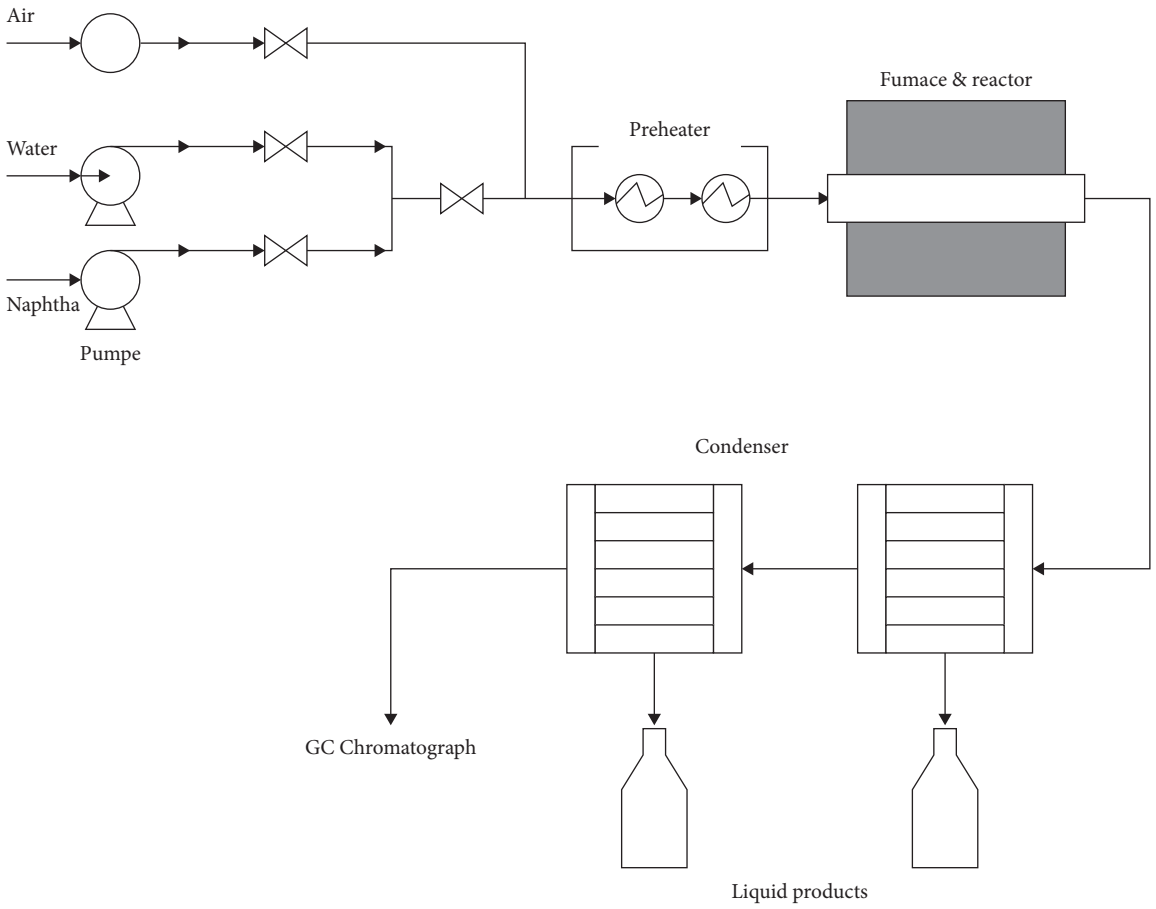

Figure 1: A pilot scale of thermal catalytic cracking setup.

Table 2: Physical properties and composition of naphtha feed.

Physical properties of naphtha				
Density (g/ml)				0.655
Initial boiling point (°C)				60.7
Final boiling point (°C)				120.3
Chemical composition (wt. %)				
Aromatic	Naphtha	Iso-paraffin	*n*-paraffin	Carbon number
0	0	0.12	2.16	C4
0	3.58	21.38	27.34	C5
1.58	3.84	12.29	10.19	C6
1.57	4.34	3.82	3.29	C7
0.55	0.92	1.2	1.04	C8
0.03	0	0.5	0.26	C9
3.73	**12.68**	**39.31**	**44.28**	**Total**

Table 3: Operational conditions for thermal catalytic cracking over SAPO-34.

Parameters	Amounts
Feed flow rate (g/min)	1.2
Ratio of hydrocarbon vapor (g/g)	0.5
Catalyst weight (g)	1
Weight hourly space velocity (WHSV, h^{-1})	12.4

Table 4: Operational conditions for thermal catalytic cracking of naphtha.

Parameters	Amounts
Feed flow rate (g/min)	2
Ratio of hydrocarbon vapor (g/g)	0.5
Catalyst weight (g)	1
WHSV (h^{-1})	60

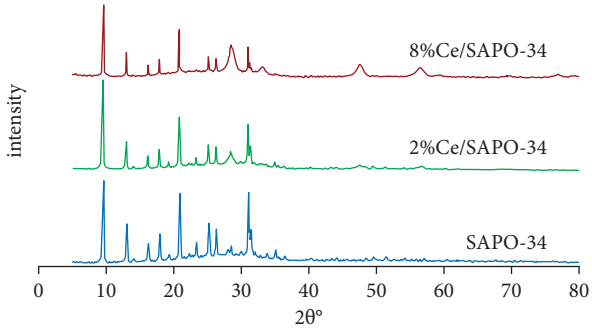

Figure 2: XRD images of SAPO-34 and Ce/SAPO-34 catalysts.

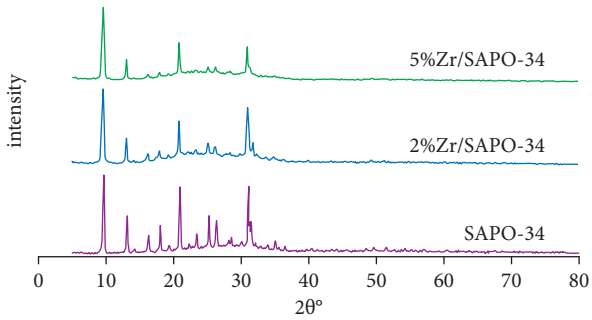

Figure 3: XRD images of SAPO-34 and Zr/SAPO-34 catalysts.

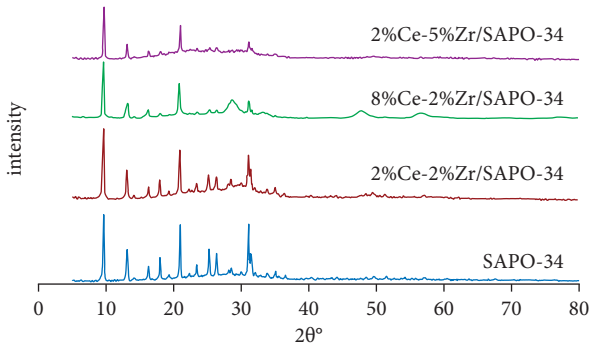

Figure 4: XRD images of SAPO-34 and Ce-Zr/SAPO-34 catalysts.

3.3. SEM Analysis of Catalyst SAPO-34. Figure 9 shows the morphology of SAPO-34, and Figures 10–12 show the morphology of 2% Ce-SAPO-34, 8% Ce-SAPO-34, and 15% Ce-SAPO-34, respectively. From Figures 10–12, it is clear that the morphology of the catalysts is preserved after modification by Ce [92–94]. In addition, Figures 13 and 14 are SEM catalysts of 2% Zr/SAPO-34 and 2% Ce-2% Zr/SAPO-34, respectively. The images also show that the morphology of the catalysts has not changed. The white particles on the catalyst surface at 500 nm can be attributed to Ce and Zr particles.

3.4. SEM Analysis of Catalyst HZSM-5. As can be seen in Figure 15, the zeolite catalyst has a spherical structure, and its particle size varies. After loading the xenolith by Ce and

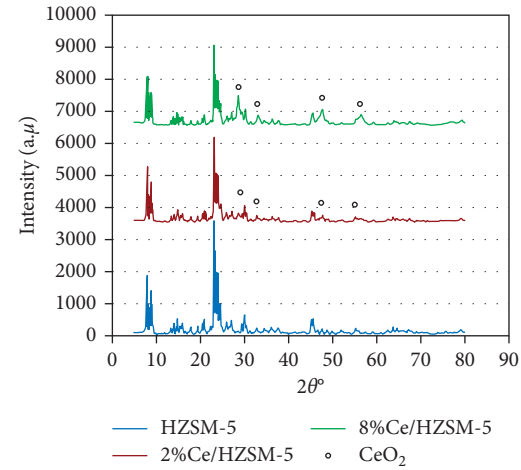

Figure 5: XRD images of HZSM-5 and Ce/HZSM-5 catalysts.

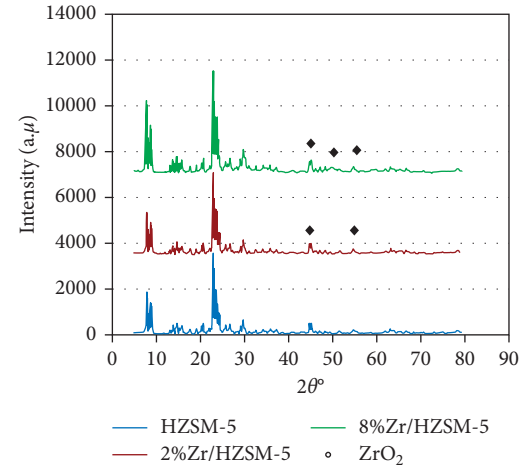

Figure 6: XRD images of HZSM-5 and Zr/HZSM-5 catalysts.

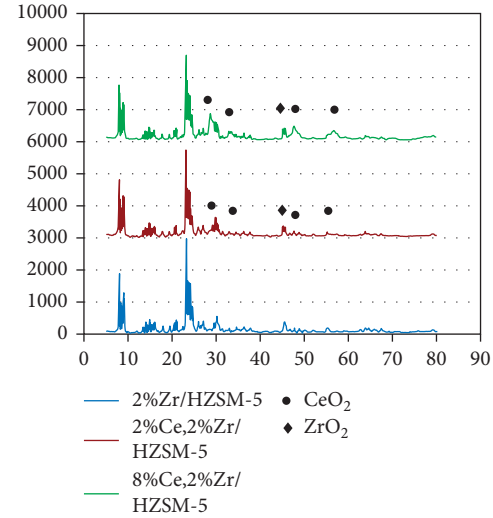

Figure 7: XRD images of HZSM-5 and Ce-Zr/HZSM-5 catalysts.

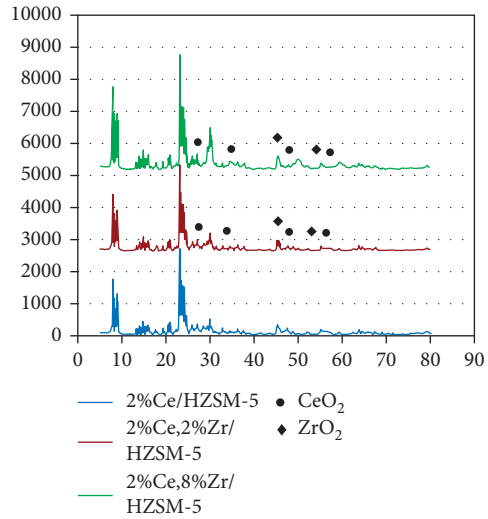

Figure 8: XRD images of HZSM-5 and Ce-Zr/HZSM-5 catalysts.

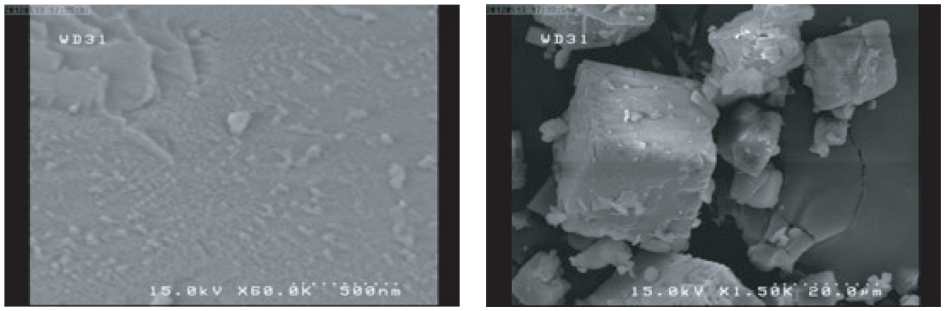

Figure 9: SEM analysis image of unmodified SAPO-34 zeolite.

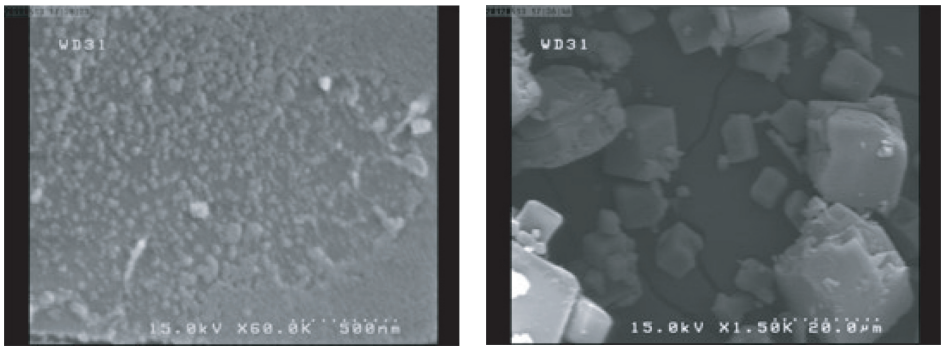

Figure 10: SEM image of 2% zeolite Ce-SAPO-34.

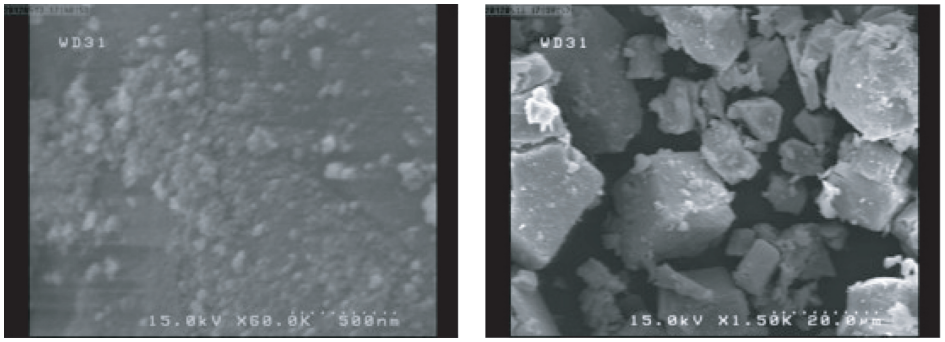

Figure 11: SEM image of 8% zeolite Ce-SAPO-34.

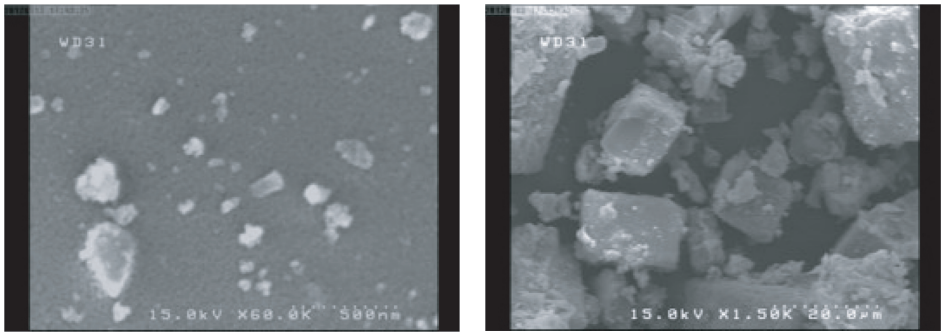

Figure 12: SEM image of 15% zeolite Ce-SAPO-34.

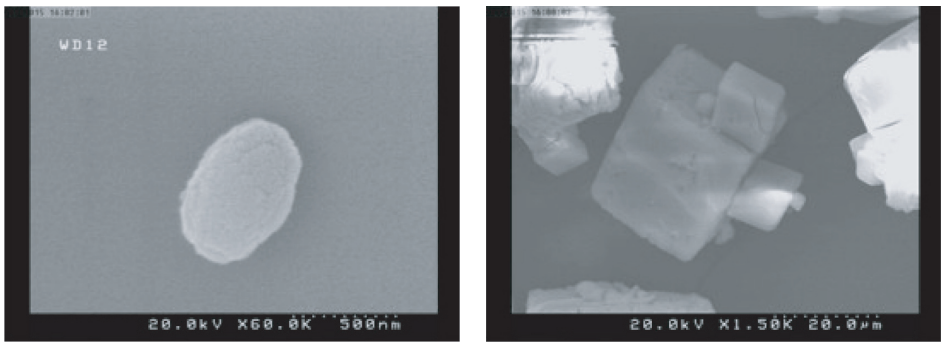

Figure 13: SEM image of 2% zeolite Zr-SAPO-34.

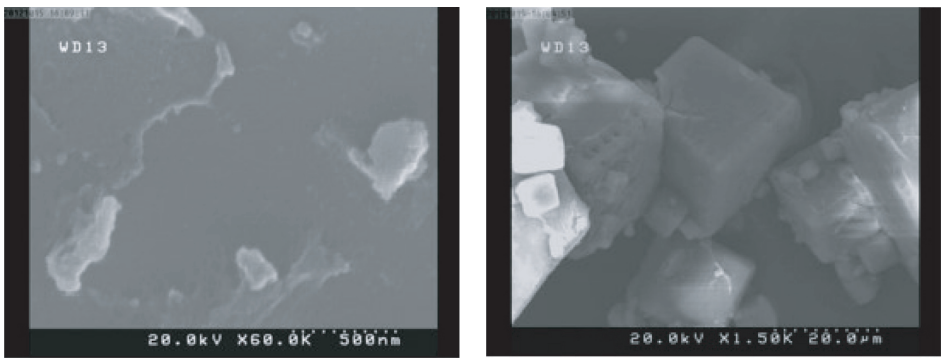

Figure 14: SEM image analysis of 2% Ce-2% Zr-SAPO-34 zeolite.

Zr salts, the spherical structure is completely preserved. By loading the zeolite catalyst with the help of Ce metal, the particles accumulate, which is visible in part B. After loading with the help of Zr metal, the dispersion of the particles increased compared to the unmodified catalyst. This scattering is well observed in part C. Simultaneous inclusion of Ce vesicles reduced the particle size. The white aggregates in part D can be attributed to Ce metal, and the smaller particles can be attributed to the presence of Ce metal [95–102].

3.5. BET Analysis of Catalysts HZSM-5 and SAPO-34. The specific surface area and volume of the catalyst cavities were measured using BET analysis, and the results are presented in Table 5. As shown in Table 5, after the modification of the SAPO-34 catalyst by Ce and Zr, the specific surface area and volume of the cavities decreased, possibly due to the penetration of CeO_2 and ZrO_2 oxides into the catalyst cavities. The BET analysis results for HZSM-5 show lower specific surface area and cavity volume for HZSM-5 than for SAPO-34, while the micro-cavity volume in HZSM-5 is significantly higher than that for SAPO-34. Thus, the results prove that the cavities in the SAPO-34 structure are predominantly micro, but in HZSM-5, the cavities are in both micro- and microforms with approximately equal volumes. In addition, the BET results for 2%Ce-2%Zr/HZSM-5 show that the specific surface area and volume of the cavities decreased to a lesser extent than those of the modified SAPO-34, due to the larger pores of HZSM-5 compared to SAPO-34 [103–105].

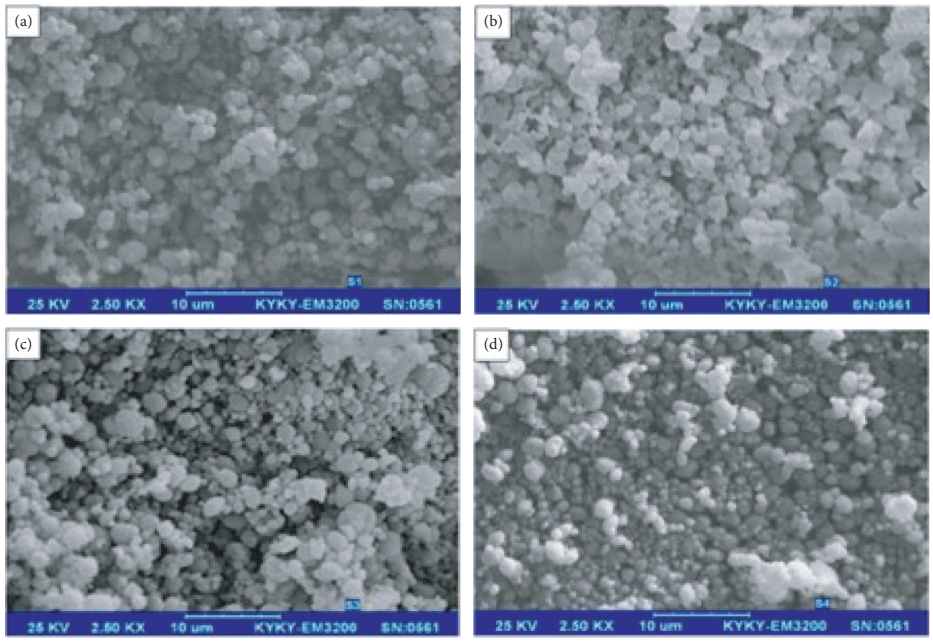

Figure 15: SEM image of (a) HZSM-5. (b) 8% Ce- HZSM-5. (c) 8% Zr- HZSM-5. (d) 8% Ce-8% Zr- HZSM-5.

Table 5: HZSM-5/SAPO-34 catalyst structural information prepared based on BET analysis.

Catalyst	BET surface area (m^2/g)	Total pore volume (cm^3/g)	Vmicro (cm^3/g)	Vmeso (cm^3/g)
SAPO-34	573	0.280	0.246	0.034
2%Ce/SAPO-34	407	0.204	0.180	0.024
8%Ce/SAPO-34	390	0.194	0.175	0.019
2%Zr/SAPO-34	392	0.185	0.164	0.021
5%Zr/SAPO-34	385	0.179	0.162	0.017
2%Ce-2%Zr/SAPO-34	417	0.237	0.206	0.031
HZSM-5	442.72	0.258	0.132	0.126
2%Ce/HZSM-5	366.65	0.220	0.069	0.151
8%Ce/HZSM-5	361.21	0.210	0.085	0.125
2%Zr/HZSM-5	375.42	0.230	0.089	0.141
8%Zr/HZSM-5	370.31	0.210	0.098	0.112
2%Ce-2%Zr/HZSM-5	386.41	0.237	0.062	0.175
2%Ce-8%Zr/HZSM-5	368.64	0.223	0.084	0.139
8%Ce-2%Zr/HZSM-5	351.89	0.195	0.092	0.103
8%Ce-8%Zr/HZSM-5	360.35	0.210	0.096	0.116

3.6. NH3-TPD Analysis of Catalyst SAPO-34. The TPD diagram of the basic SAPO-34 catalysts and the modified SAPO-34 catalysts with Ce and Zr metals is shown in Figure 16. The values of NH_3 absorbed per unit weight of catalyst are also given in Table 6. As shown in Figure 16, the NH_3-TPD diagrams of all samples show two peaks at temperatures of about 150°C and 450°C. The first peak is related to the hydroxyl groups P-OH, Si-OH, and Al-OH, and these hydroxyl groups are usually attributed to weak acids. The peak at 450°C belongs to the Si-OH-Al hydroxyl groups, which attribute the hydroxyl groups to the strong acids. As can be seen in Figure 16 and Table 6, the amount of total acidity increased with the addition of Ce to the catalyst, and the total acidity decreased with the addition of Zr. But generally after loading Ce and Zr metals, in all modified catalysts, the number of strong acid centers increased compared to the basal state, and this increase was greater in the catalysts modified by the synergy of Ce and Zr. In general, the presence of empty f orbitals in Ce creates new Lewis acid sites and increases the total number of acid centers. Improvement of the catalyst with the Zr element causes the Ce oxide to sit on the outer surface of the catalyst and to destroy some of the surface acid sites on the outer surface of the catalyst. Therefore, the weak acidity density decreases after the catalyst modification with Zr. It should be noted, however, that there is an optimum value for this increase in acidity as the density of the acid centers increases, and their adverse hydrogen transfer reactions increase.

3.7. NH3-TPD Analysis of Catalyst HZSM-5. In Figure 17 and Table 7, the effect of Ce metal loading on acidity has been investigated by TPD analysis. As expected, Ce metal

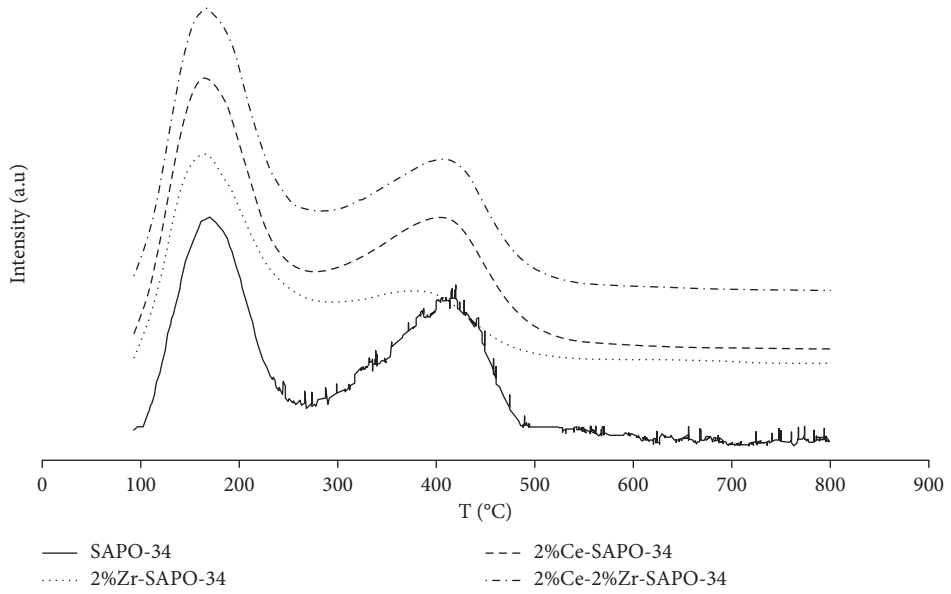

Figure 16: NH3-TPD analysis of the effect of increasing Ce and Zr metals on SAPO-34 catalyst.

Table 6: Acid properties of catalysts NH3-TPD analysis.

Catalysts	Acidity (mmol NH3/g-catalyst)		
	Weak acid	Middle and strong acid	Total acid
SAPO-34	0.625	0.702	1.327
2%Ce-SAPO-34	0.677	0.942	1.619
2%Zr-SAPO-34	0.358	0.843	1.201
2%Ce-2%Zr-SAPO-34	0.725	0.973	1.698

increased the acidity of zeolite. Increased acidity has occurred for both strong and weak acid centers. The reason for this can be attributed to the polarization of the Si-OH and AL-OH bonds by the quantitation and induction of Ce, which leads to an increase in electron density and an increase in acidic strength. The number of Lewis acids also increases due to the empty orbital f of Ce. Generally, this is expected for rare earth metals except for Ga [106–110]. Moving the location of the cycads to lower temperatures after Ce loading for weak acids indicates a decrease in the strength of these acids, and the transfer of the pics after Ce loading for the strong acids indicates an increase in the strength of these acids. The TPD analysis to investigate the loading of Zr metal is shown in Figure 18 and Table 7. Zr metal loading is particularly important in strong acidic surfaces. The increase in the number of weak and strong acid sites as well as the transfer of these peaks to higher temperatures indicating increased acidic strength can be well illustrated in these graphs. The simultaneous increase of Ce vesicles over a cone on the base catalyst has reduced the acidity. This decrease is evident from the results of the TPD analysis in Figure 19, Table 7.

3.8. TGA Analysis of Catalysts HZSM-5 and SAPO-34. To check the amount of coke sitting on the catalysts, TGA analysis was performed on the samples at temperatures up to 900°C. The results of the TGA analysis are presented in Figure 20. Weight loss of samples up to 250°C can be attributed to moisture removal from the catalyst structure, and weight loss at higher temperatures is due to the burning of coke sitting on the catalyst structure. According to TGA results, weight loss at temperatures above 250°C for SAPO-34, 2% Ce-2% Zi/SAPO-34, HZSM-5, and 2% Ce-2% Zi-HZSM-5 catalysts, respectively, is equal to 8.3%, 6.42%, 5.66%, and 4.26%, respectively, which are in harmony with the reduction of ethylene yields and especially propylene on the catalysts.

4. Catalyst Performance

4.1. Results of Thermal Catalytic Cracking of Naphtha Catalyst SAPO-34. The results of the thermal catalytic cracking of Naphtha reactions on the SAPO-34 catalytic base with Ce, Ce and Zr and Zr elements are visible in Tables 8 and 9, respectively. In addition, to compare the yields of ethylene and propylene on the catalysts, the results can be seen in Figures 21 and 22 through Figure 23. Reactor results show an increase in the efficiency of light olefins in the catalytic thermal catalytic cracking of Naphtha process on the SAPO-34 catalyst compared to the catalytic thermal catalytic cracking of Naphtha process, so that the yields of Light olefins were 2.94 and 6.92% by SAPO -34 increase. Adding 2% Ce and 2% Zr significantly increased the yield of ethylene and propylene. This increase in the yield of ethylene and propylene can be attributed to the increased acidity of the catalyst. According to the NH3-TPD analysis results, the strong acidity of the catalysts increased by 2% Ce-2% Zr/SAPO-34 > 2% Ce/SAPO-34 > 2% Zr/SAPO-34> SAPO-34, respectively, and the reactor results also show the same ranking in ethylene and propylene yields, with SAPO-34 having the lowest yield and 2% Ce-2% Zr/SAPO-34 having the highest yield of light olefins. As the results show, further

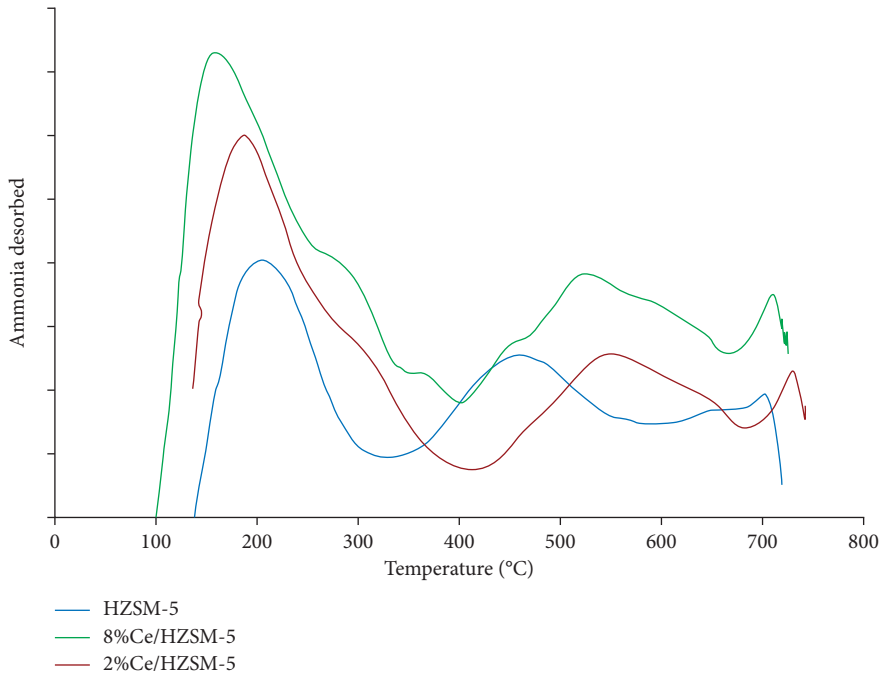

Figure 17: NH3-TPD analysis of the effect of Ce loading on acidic properties of HZSM-5.

Table 7: Acid properties of catalysts NH3-TPD analysis.

Catalysts	Acidity (mmol NH3/g-catalyst)		
	Weak acid	Middle and strong acid	Total acid
HZSM-5	0.40	0.82	1.18
2%Ce- HZSM-5	0.72	0.85	1.57
8% Ce - HZSM-5	1.05	1.49	2.54
2%Zr- HZSM-5	0.53	1.03	1.55
8%Zr- HZSM-5	0.71	1.33	2.04
2%Ce-8%Zr- HZSM-5	0.27	0.14	0.41
8%Ce-2%Zr- HZSM-5	0.18	0.00	0.18

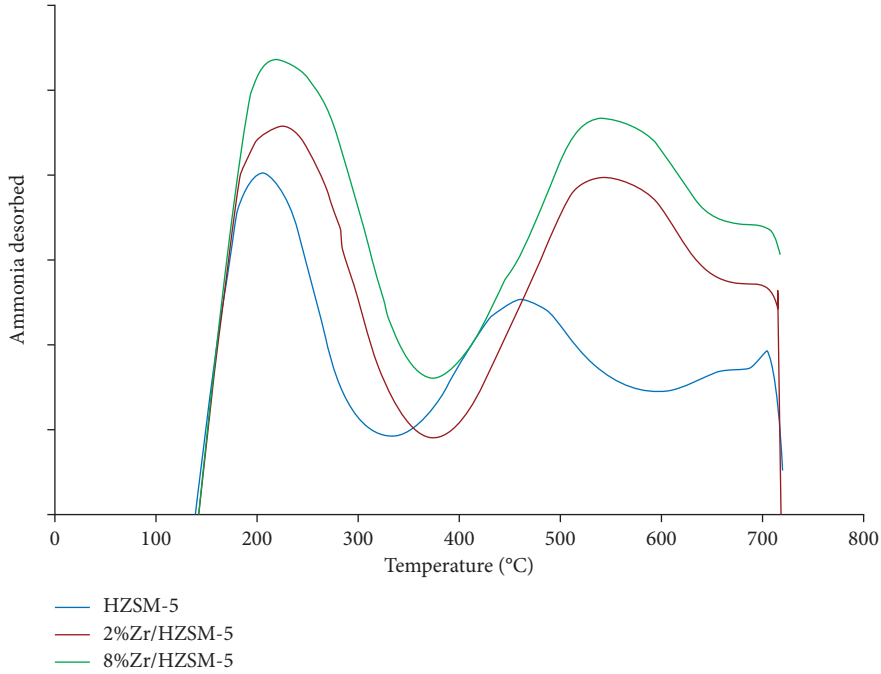

Figure 18: NH3-TPD analysis of the effect of Zr loading on acidic properties of HZSM-5.

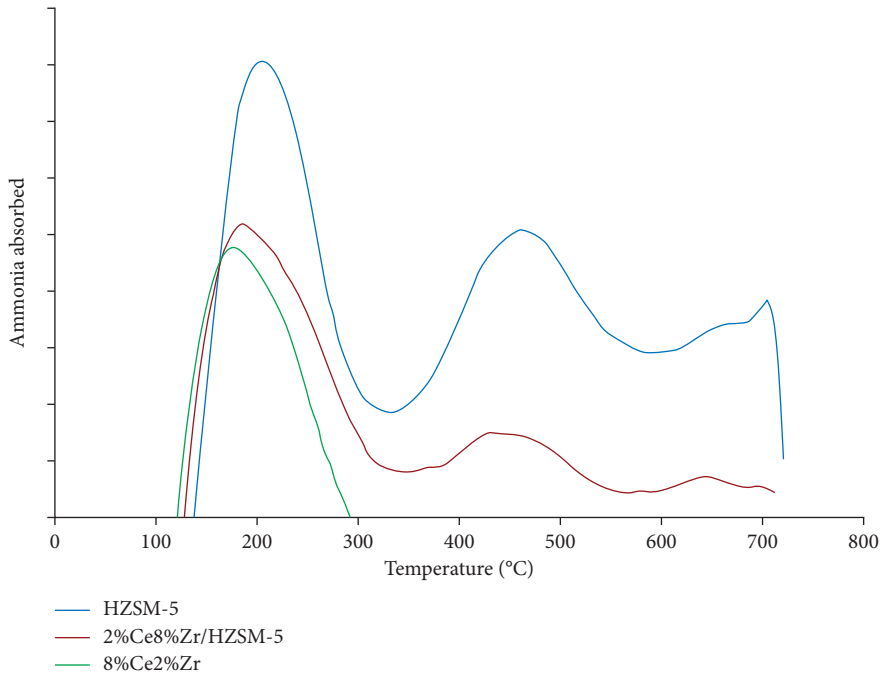

Figure 19: NH3-TPD analysis of the effect of Ce and Zr loading on acidic properties of HZSM-5.

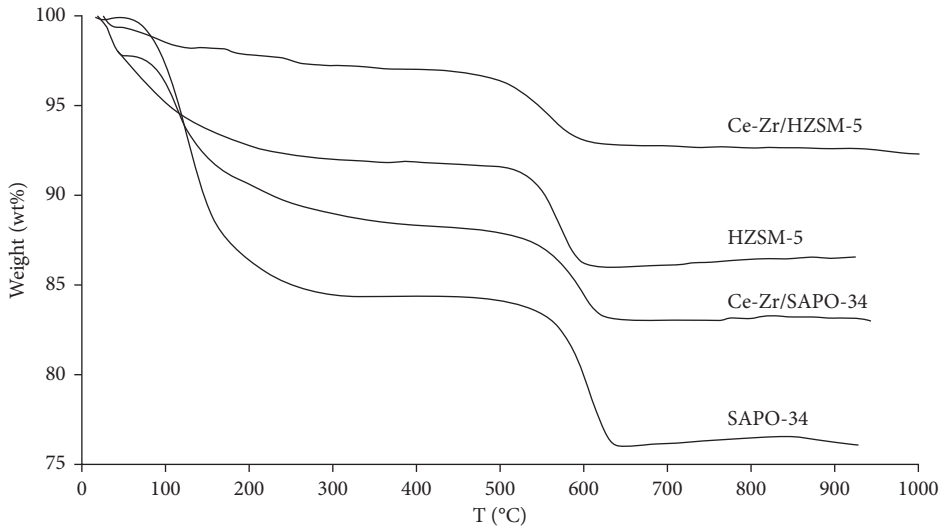

Figure 20: TGA analysis of the catalysts after the reaction.

increase in Ce and Zr loading reduces the yield of ethylene and propylene. This can be attributed to the increase in the amount of Ce and Zr oxides on the catalyst surface and the blocking of the catalyst cavities, preventing the penetration of naphtha molecules into the catalyst cavities and preventing thermal catalytic cracking of Naphtha reactions [111–115].

4.2. Results of Thermal Cracking Catalytic of Naphtha Catalyst HZSM-5. To investigate the effect of loading of Ce and Zr on the zeolite catalyst in thermal catalytic cracking of naphtha, experiments were performed according to Tables 9 and 10. In both experiments, the catalyst was added to the reactor twice, and the experiments were carried out at the operating conditions of Table 4 and the space velocity 60 h^{-1}. The results of the experiment are visible at 650°C in Figure 24 and for 750°C in Figure 25. In molecular sieving catalysts, acid sites are active sites [116–120]. It can be seen from the data in Table 7 that, with increasing base catalyst loading with Ce and Zr metals, the acidic site increased. As a result, increased production of propylene can be attributed to the sites created. According to Figures Tables 10 and 11, for propylene with increasing temper nature, some catalysts show

Table 8: Results of thermal catalytic cracking of naphtha on Ce-SAPO-34 at 750°C.

Catalytic	Yield (wt. %)					
	Methane	Ethan	Ethylene	Propylene	Butylene	C_5^+
SAPO-34	6.11	3.94	17.05	19.82	2.37	40.17
2%Ce/SAPO-34	6.9	4.61	19.69	21.26	2.42	35.55
8%Ce/SAPO-34	6.67	4.39	19.24	20.46	3.09	36.24
15%Ce/SAPO-34	6.53	4.18	18.21	19.07	2.74	38.71

Table 9: Results of thermal catalytic cracking of naphtha on Zr -SAPO-34 at 750°C.

Catalytic	Yield (wt. %)					
	Methane	Ethan	Ethylene	Propylene	Butylene	C_5^+
SAPO-34	6.11	3.94	17.05	19.82	2.37	40.17
2%Zr/SAPO-34	6.53	4.07	18.85	20.18	2.39	37.51
5%Zr/SAPO-34	6.58	3.56	19.91	18.37	2.64	38.26
8%Zr/SAPO-34	5.61	3.29	17.84	17.23	2.44	46.67

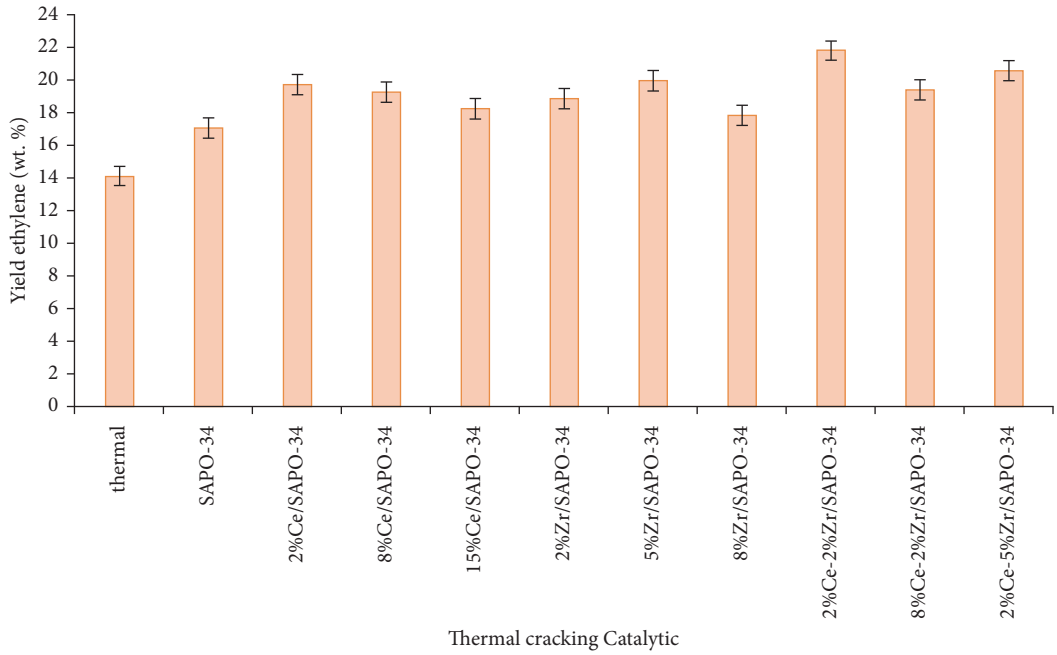

Figure 21: Comparison of ethylene yields produced by thermal catalytic cracking of naphtha.

increased efficiency, and some decrease efficiency. For catalysts with high acidity, the reduction in specific yields is significant. As can be seen, the formation of carbon ions on acidic sites increased the yield of propylene at a rate of bending [37, 121–124].

4.3. The Effect of Loading Ce. According to the results presented for catalysts modified with 2% and 8% Ce, the yield of light olefins increases with the addition of this element on zeolite. The results for the efficiency of these catalysts in Figure 26 are shown for both temperatures. According to the results presented in Figure 26, with Ce metal loading the ethylene yield, increased compared to the propylene yield and with the Ce loading, the propylene yield increased significantly. By comparing the propylene yields at the two reaction temperatures, we find that, by increasing the 700°C, the propylene yields decrease. Since propylene is an intermediate material, an increase in temperature increases secondary reactions. As the acid centers are close to each other, and the acidity increases, at high temperatures, the hydrogen transfer reactions accelerate, reducing the saturation of propylene and reducing its efficiency. In Table 12, the rate of change in yields of light olefins after the addition of Ce metal to the base catalyst is visible.

4.4. The Effect of Loading Zr. As shown in Figure 27, the ethylene yield did not change much with the addition of Zr to the zeolite. The highest yield was related to 2% Zr loading, which increased the total production of olefins by 40%. This increase can be attributed to the catalytic acidity change.

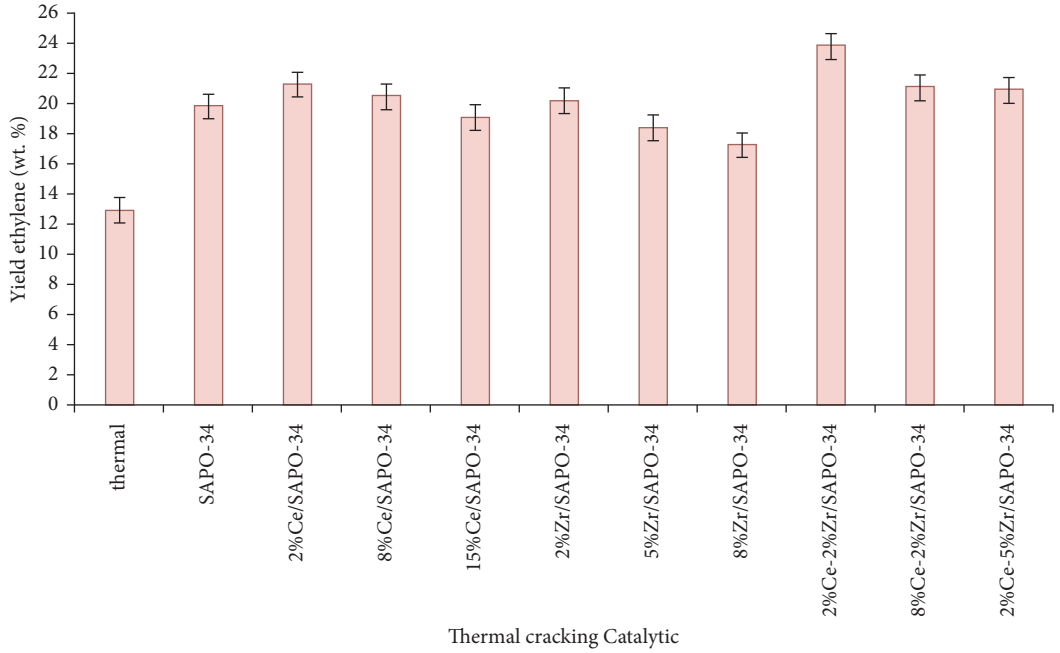

Figure 22: Comparison of propylene yields produced by thermal catalytic cracking of naphtha.

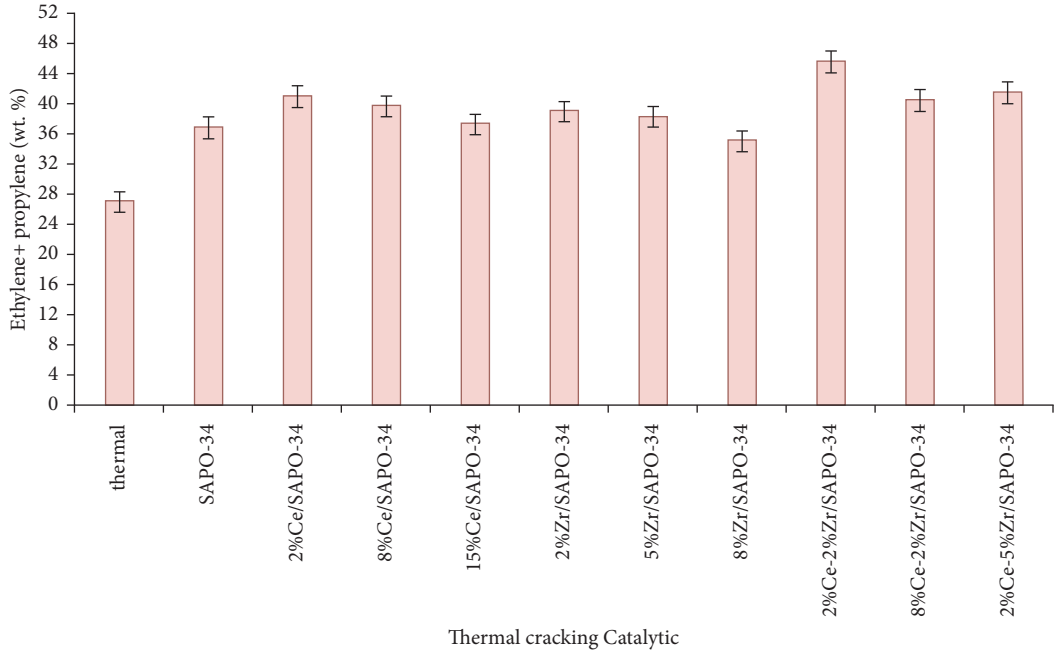

Figure 23: Comparison of ethylene + propylene yields produced by thermal catalytic cracking of naphtha.

According to the results of Table 7, the loading of Zr catalyst increases with increasing acidity, and on the other hand, the strength of weak acids also increases, making it easier to break down and increase efficiency. But on the other hand, increasing acidity, especially at the surface, speeds up secondary reactions and reduces the efficiency of olefins. Therefore, catalysts with moderate acid sites have higher efficiency in this process. In Table 13, the rate of change in yields of light olefins after the addition of Zr metal to the base catalyst is observable.

4.5. Catalytic Stability Is Investigated. In the previous sections, the effects of SAPO-34 and HZSM-5 with different modifications on the efficiency of light olefins were investigated. However, it should be noted that the catalyst is

Table 10: The results of thermal catalytic cracking of naphtha at 650°C.

Yield					Product name
8%Zr/HZSM-5 650°C	2%Zr/HZSM-5 650°C	8%Ce/HZSM-5 650°C	2%Ce/HZSM-5 650°C	HZSM-5 650°C	
6.60	6.80	7.21	9.34	8.47	Methane
3.53	3.14	3.85	4.04	3.01	Ethane
17.31	18.93	17.85	16.99	15.87	Ethylene
2.57	2.40	2.84	2.20	1.10	Propane
30.0	22.64	29.11	24.82	20.85	Propylene
0.33	0.48	1.35	1.08	0.10	i-butane
0.10	0.17	1.32	1.03	0.04	*n*-butane
0.20	0.75	1.67	1.54	0.42	Propadien
2.94	2.98	4.22	3.83	2.74	Acetylene
0.69	3.72	1.91	1.57	0.56	T2-butene
3.22	3.41	4.10	4.94	3.81	1-butene
3.21	0.90	1.27	0.94	0.0	Iso-butene
0.21	0.19	1.40	1.18	0.10	C2-butene
0.06	0.07	1.32	1.00	0.03	*n*-pentane
0.83	1.79	2.41	2.18	1.17	MA
0.58	0.88	2.15	2.67	1.93	Hydrogen
25.78	33.03	25.67	19.89	38.00	C^+

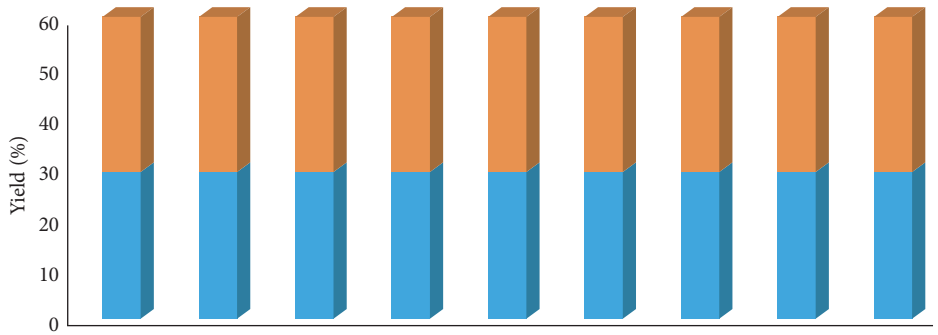

	HZSM-5	2%Ce/H ZSM-5	8%Ce/H ZSM-5	2%Zr/H ZSM-5	8%Zr/H ZSM-5	2%Ce 2%Zr/H ZSM-5	2%Ce8 %Zr/H ZSM-5	8%Ce2 %Zr/H ZSM-5	8%Ce8 %Zr/H ZSM-5
Propylene	34	40	46	50	45	32	34	28	29
Ethylene	14	15	16	17	15	14	15	13	11

Figure 24: Comparison of modified olefin catalyst yields at 650°C.

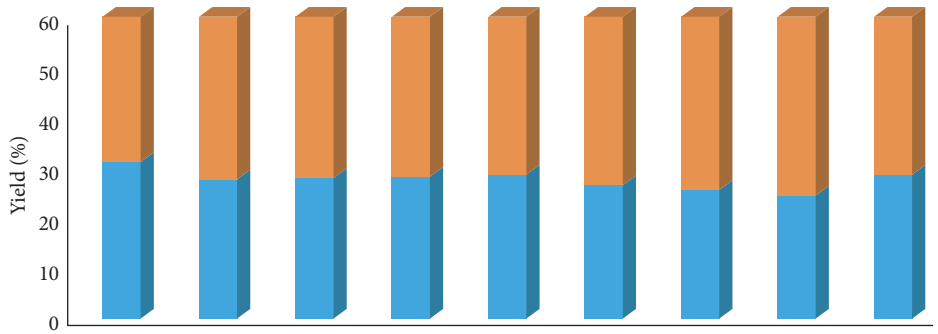

	HZSM-5	2%Ce/H ZSM-5	8%Ce/H ZSM-5	2%Zr/H ZSM-5	8%Zr/H ZSM-5	2%Ce 2%Zr/H ZSM-5	2%Ce8 %Zr/H ZSM-5	8%Ce2 %Zr/H ZSM-5	8%Ce8 %Zr/H ZSM-5
Propylene	40	42	44	46	40	39	38	37	40
Ethylene	18	16	17	18	16	14	13	12	16

Figure 25: Comparison of modified olefin catalyst yields at 700°C.

Table 11: The results of thermal catalytic cracking of naphtha at 700°C.

Yield					Product name
8%Zr/HZSM-5 700°C	2%Zr/HZSM-5 700°C	8%Ce/HZSM-5 700°C	2%Ce/HZSM-5 700°C	HZSM-5 700°C	
6.66	6.94	9.92	9.81	10.41	Methane
3.56	3.21	4.30	4.25	3.71	Ethane
19.92	19.10	19.06	18.84	19.29	Ethylene
2.60	2.45	2.34	2.31	1.35	Propane
27.60	21.96	26.47	26.59	22.64	Propylene
0.33	0.49	1.14	1.13	0.13	i-Butane
0.20	0.17	1.09	1.08	0.05	*n*-Butane
0.21	0.76	1.64	1.62	0.52	Propadien
2.97	3.04	4.07	4.02	0.37	Acetylene
3.70	1.74	1.66	1.64	0.69	T2-Butene
3.25	3.48	5.26	5.19	4.69	1-Butene
3.25	0.92	1.00	0.99	0	Iso-butene
0.21	0.19	1.25	1.24	0.12	C2-Butene
0.06	0.08	1.07	1.05	0.04	*n*-Pentane
0.84	1.83	2.31	2.28	1.43	MA
0.59	0.90	2.83	2.80	2.38	Hydrogen
25.61	35.60	17.94	18.93	31.97	C^+

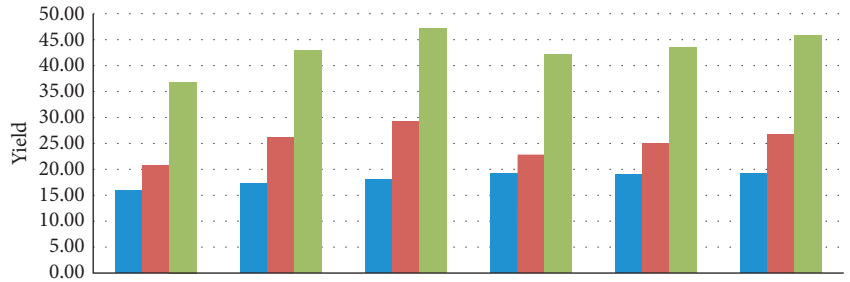

	HZSM-5 (650°C)	2%Ce/HZSM-5 (650°C)	8%Ce/HZSM-5 (650°C)	HZSM-5 (700°C)	2%Ce/HZSM-5 (700°C)	8%Ce/HZSM-5 (700°C)
Propylene	15.87	16.99	17.85	19.29	18.84	19.06
Ethylene	20.85	25.82	29.11	22.64	24.59	26.47
Ethylene+ Propylene	36.72	42.81	46.96	41.93	43.43	45.53

Figure 26: Ce loading effect on the yield of light olefins.

Table 12: Percentage of olefin yield changes after Ce loading.

No.	Cerium loading percentage	Temperature (°C)	Yield		
			Ethylene	Propylene	Ethylene + propylene
1	2	650	7.06	23.83	16.58
2	8	650	12.46	39.62	27.88
3	2	700	2.3	8.61	3.57
4	8	700	1.19	16.93	8.89

suitable for the thermal catalytic cracking of naphtha of hydrocarbons, which, in addition to increasing the yield of light olefins, has good stability. One of the problems for catalysts for industrial applications is their inactivation due to the formation of coke on active sites. Zeolite catalysts are usually inactive due to the formation of coke and the removal of aluminum from the fast zeolite structure and need to be revived. Therefore, many studies have focused on the modification of these catalysts to maintain good stability. In this section, to investigate the

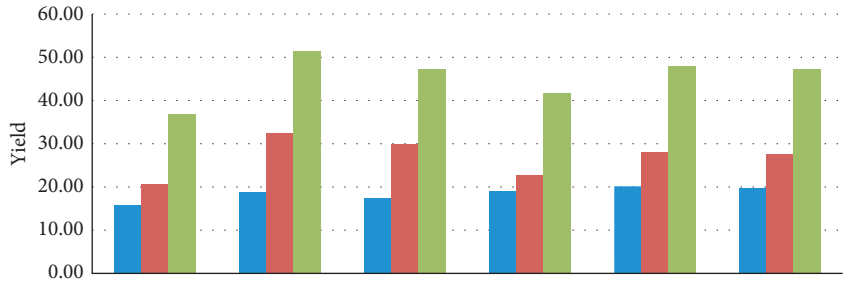

	HZSM-5 (650°C)	2%Zr/ HZSM-5 (650°C)	8%Zr/ HZSM-5 (650°C)	HZSM-5 (700°C)	2%Zr/ HZSM-5 (700°C)	8%Zr/ HZSM-5 (700°C)
Ethylene	15.87	18.93	17.31	19.29	20.10	19.62
Propylene	20.85	32.64	30.00	22.64	27.96	27.60
Ethylene+ Propylene	36.72	51.57	47.31	41.93	48.05	47.22

Figure 27: Zr loading effect on the yield of light olefins.

Table 13: Percentage of olefin yield changes after Zr loading.

No.	Cerium loading percentage	Temperature (°C)	Yield		
			Ethylene	Propylene	Ethylene + propylene
1	2	650	19.28	56.53	40.43
2	8	650	9.08	43.88	28.84
3	2	700	4.18	23.48	14.6
4	8	700	1.17	21.9	12.61

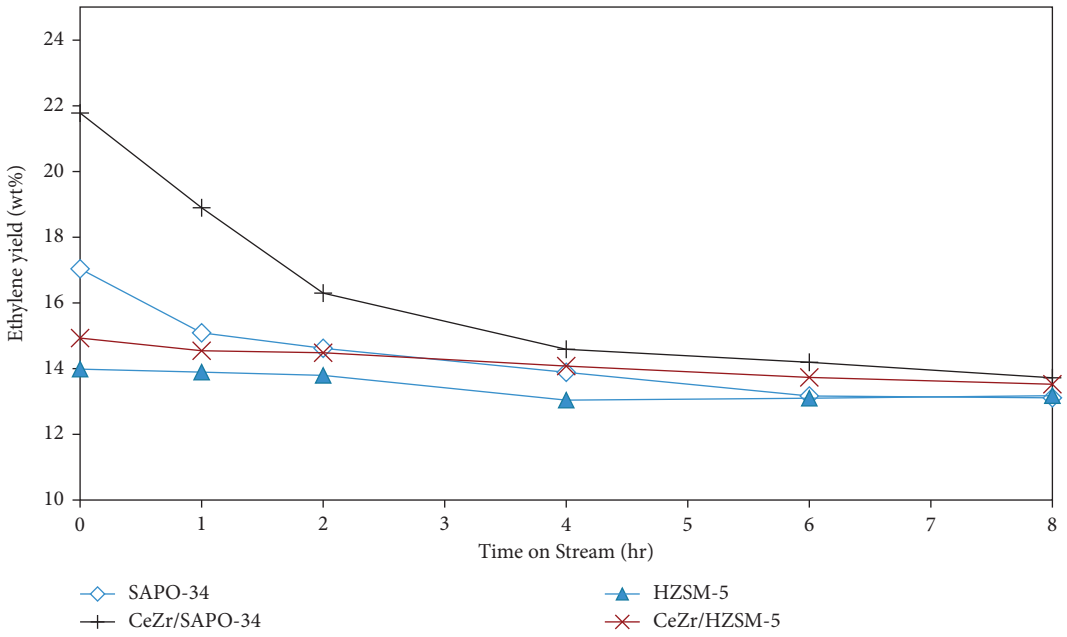

Figure 28: Results of ethylene production efficiency with increasing reaction time.

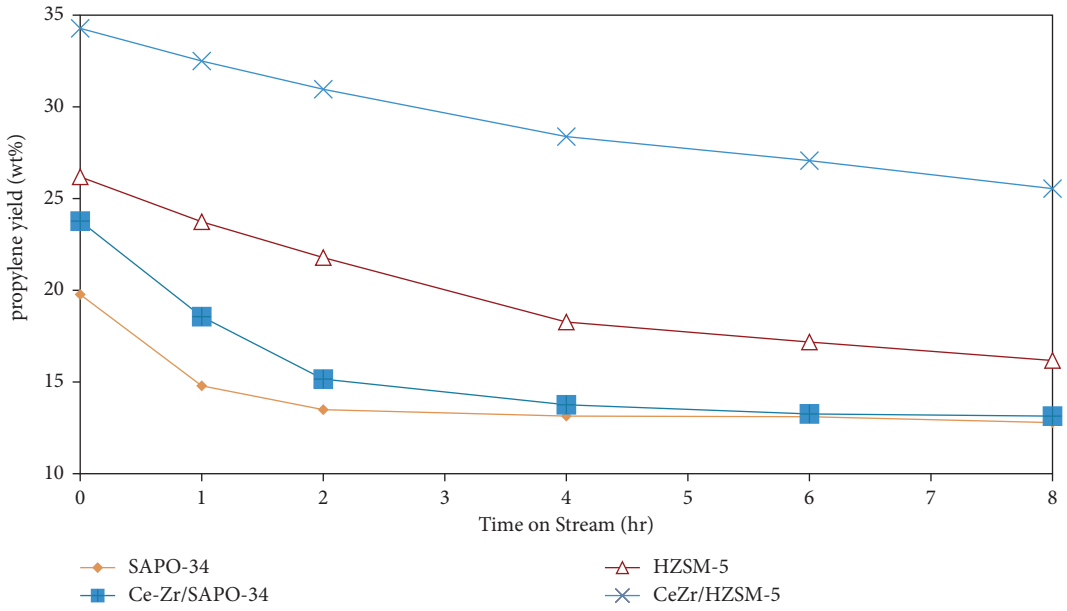

Figure 29: Results of propylene production efficiency with increasing reaction time.

Table 14: Research on thermal catalytic cracking of naphtha unit.

Yield wt. %			Temperature operating (°C)	Size mesh	Catalyst type		Years	References
Ethylene + propylene	Propylene	Ethylene			Active element	Basic		
31.84	12.78	19.06	628	10–25	Fe	CNT	2012	[125]
42.29	22.86	19.43	680	10–25	Ce-La-Mo	ZSM-5	2010	[83]
52.5	36	16.5	680	10–25	Ce	ZSM-5	2010	[84]
49.36	22.56	26.8	750	10–25	Ce-La	SAPO-34	2012	[90]

stability of catalysts, in the experiment, SAPO-34, 2% Ce-2% Zr/SAPO-34, HZSM-5, and 2% Ce2-2% Zr- HZSM-5 were administered for 8 hours. The result of this experiment is shown for the ethylene yield in Figure 28 and for the propylene yield in Figure 29.

Figure 29 shows that the yields of ethylene catalysts of HZSM-5 and 2% Ce-2% Zr/HZSM-5 did not change significantly over time and remained at about 14 wt%. The results show that, after 2 h of ethylene yield reaction on SAPO-34, the catalyst is inactivated to its minimum level. The 2% Ce-2% Zr/SAPO-34 catalyst showed significantly better performance and increased catalyst inactivation time. As shown in Figure 29, the propylene yields decreased by 6.36% and 8.66%, respectively, while propylene yields decreased on the SAPO-34 and 2% Ce-2% Zr-SAPO-34 catalysts, respectively, while decreasing the propylene efficiency, respectively. The HZSM-5 catalyst, and especially the 2% Ce-2% Zr/HZSM-5 catalyst, was much lower than SAPO-34 within 2 hours. It is also apparent that SAPO-34 is almost deactivated during the first 2 hours if the performance of the HZSM-5 catalyst is significantly better than that of SAPO-34.

4.6. Comparison of Results with Other Similar Studies. Further research has been conducted on the thermal catalytic cracking of Naphtha at various universities. This article was conducted in a thermal catalytic cracking of Naphtha unit located in the Iranian Olefin Research Laboratory, and most of them, the reactor conditions, vapor to hydrocarbon ratio, residence time, catalyst weight, feed flow type, and intensity, were the same. The operating conditions, the type of catalyst, and the results of the studies are presented in Tables 13 and 14.

5. Conclusion

In this paper, SAPO-34 zeolites were used as catalysts for the production of Ethylene, propylene in the thermal catalytic cracking of Naphtha process. The results of the thermal catalytic cracking of Naphtha using the above catalyst showed an increase in the efficiency of the lightweight primers compared to the thermal catalytic cracking of naphtha at the same temperature. To further enhance the efficiency of light olefins, SAPO-34 was modified using Ce and Zi elements. SEM and XRD analyses were performed on some modified samples, and the results showed that the catalyst structure was not damaged after the addition of Ce and Zi. The results of the NH3-TPD analysis showed that the strong acidity of the catalyst increased after modification by Ce and Zr. Reactor results showed that the yield of light olefins increased after modification by Ce and Zr, and the highest olefin yields were obtained on catalysts with low

synergies of Ce and Zr. Comparing the performance of SAPO-34, experiments were performed under similar conditions based on HZSM-5, which is known as a reference catalyst in the thermal catalytic cracking of naphtha process. The results showed that although the yield of ethylene on SAPO-34 catalysts was higher than that of HZSM-5, propylene and total olefin production were higher than the on HZSM-5 catalyst. The stability test results showed better performance of HZSM-5 catalyst against SAPO-34. Also the stability test results showed that the performance of both SAPO-34 and HZSM-5 catalysts improved after modification with Ce and Zi.

Based on these experiments, the main results are summarized as follows:

(1) Conservation of both Catalysts structures after modification with Ce and Zi elements

(2) Increased strong acidity of SAPO-34 after modification with Ce and Zi elements

(3) Increased ethylene and propylene yields on SAPO-34 compared with thermal cracking

(4) Increased ethylene and propylene yields after modification of SAPO-34 with cerium and zirconium elements

(5) Higher ethylene yields on SAPO-34 and higher propylene yields on HZSM-5

(6) ZSM-5 has better stableness than SAPO-34

(7) Increased stability of both catalysts after modification with Ce and Zi elements

Data Availability

No data were used to support this study.

Consent

Additional informed consent was obtained from all individual participants for whom identifying information is included in this paper.

Disclosure

The funders had no role in the design of the study; in the collection, analyses, or interpretation of data; in the writing of the manuscript, or in the decision to publish the results. The study submitted is part of the authors' doctoral thesis.

Conflicts of Interest

The authors declare that they have no conflicts of interest.

References

[1] M. Izadi, "Propylene production considerations," *Journal of Petroleum*, vol. 72, pp. 16–21, 2009.

[2] Y. Yoshimura, N. Kijima, T. Hayakawa et al., "Catalytic cracking of naphtha to light olefins," *Catalysis Surveys From Japan*, vol. 4, pp. 157–168, 2000.

[3] Z. Lu, F. Zhang, H. Fu, H. Ding, and L. Chen, "Rotational nonlinear double-beam energy harvesting," *Smart Materials and Structures*, vol. 31, 2021.

[4] A. Chauvel and G. Lefebvre, "Petroleum processes," *OR Tech*, vol. 118, pp. 169–227, 1989.

[5] T. Ren, M. Patel, and K. Blok, "Olefins from conventional and heavy feedstocks: energy use in steam cracking and alternative processes," *Energy*, vol. 31, no. 4, pp. 425–451, 2006.

[6] M. Salimi, V. Pirouzfar, and E. Kianfar, "Enhanced gas transport properties in silica nanoparticle filler-polystyrene nanocomposite membranes," *Colloid & Polymer Science*, vol. 295, pp. 215–226, 2017.

[7] E. Kianfar, "Synthesis and characterization of AlPO4/ZSM-5 catalyst for methanol conversion to dimethyl ether," *Russian Journal of Applied Chemistry*, vol. 91, pp. 1711–1720, 2018.

[8] E. Kianfar, "Ethylene to propylene conversion over Ni-W/ZSM-5 catalyst," *Russian Journal of Applied Chemistry*, vol. 92, pp. 1094–1101, 2019.

[9] N. Rane, M. Kersbulck, R. A. van Santen, and E. J. M. Hensen, "Cracking of n-heptane over Brønsted acid sites and Lewis acid Ga sites in ZSM-5 zeolite," *Microporous and Mesoporous Materials*, vol. 110, no. 2-3, pp. 279–291, 2008.

[10] M. J. Tallman, "Catalytic routes to olefins," in *Proceedings of the 2008 AIChE Spring Meeting and Global Congress on Process Safety*, New Orleans, Louisiana, April 2008.

[11] J. S. Plotkin, "The changing dynamics of olefin supply/demand," *Catalysis Today*, vol. 106, pp. 10–14, 2005.

[12] N. Rahimi and R. Karimzadeh, "Catalytic cracking of hydrocarbons over modified ZSM-5 zeolites to produce light olefins: a review," *Applied Catalysis A: General*, vol. 398, no. 1-2, pp. 1–17, 2011.

[13] J.-H. Kim, A. Ishida, M. Okajima, and M. Niwa, "Modification of HZSM-5 by CVD of various silicon compounds and generation of para-selectivity," *Journal of Catalysis*, vol. 161, no. 1, pp. 387–392, 1996.

[14] A. Corma, "Transformation of hydrocarbons on zeolite catalysts," *Catalysis Letters*, vol. 22, no. 1-2, pp. 33–52, 1993.

[15] G. C. Smith, "Catalytic cracking of n-alkanes and n-alkylbenzenes over HZSM-5 zeolite," Dissertation, Massachusetts Institute of Technology, MA, USA, 1993.

[16] M. al Wabi, *Conversion Of Methanol To Light Olefins On Sapo -34 Kinetic Modeling And Reactor Design*, Submitted to Texas A&M University, TX, USA, 2003.

[17] M. Kim and H.-J. Chae, "Attrition resistance and catalytic performance of spray-dried SAPO-34 catalyst for MTO process: effect of catalyst phase and acidic solution," *Journal of Industrial and Engineering Chemistry*, vol. 17, pp. 621–627, 2011.

[18] E. Kianfar, "Ethylene to propylene over zeolite ZSM-5: improved catalyst performance by treatment with CuO," *Russian Journal of Applied Chemistry*, vol. 92, pp. 933–939, 2019.

[19] E. Kianfar, M. Shirshahi, and F. Kianfar, "Simultaneous prediction of the density, viscosity and electrical conductivity of pyridinium-based hydrophobic ionic liquids using artificial neural network," *Silicon*, vol. 10, pp. 2617–2625, 2018.

[20] M. Salimi, V. Pirouzfar, and E. Kianfar, "Novel nanocomposite membranes prepared with PVC/ABS and silica nanoparticles for C2H6/CH4 separation," *Polymer Science - Series A*, vol. 59, pp. 566–574, 2017.

[21] K. Y. Lee, H. Chae, and G. Seo, "Effect of crystallite size of SAPO-34 catalysts on their induction period and deactivation in methanol-to-olefin reactions," *Applied Catalysis A: General*, vol. 369, pp. 60–66, 2009.

[22] N. Xue, X. Chen, L. Nie et al., "Understanding the enhancement of catalytic performance for olefin cracking: hydrothermally stable Acids in P/HZSM -5," *Journal of Catalysis*, vol. 248, pp. 20–28, 2007.

[23] V. A. Kumara, K. K. Pant, and D. Kunzru, "Potassium-containing calcium aluminate catalysts for pyrolysis of N-heptane," *Applied Catalysis A*, vol. 162, pp. 193–200, 1997.

[24] F. Kianfar and E. Kianfar, "Synthesis of isophthalic acid/aluminum nitrate thin film nanocomposite membrane for hard water softening," *Journal of Inorganic and Organometallic Polymers*, vol. 29, pp. 2176–2185, 2019.

[25] E. Kianfar, R. Azimikia, and S. M. Faghih, "Simple and strong dative attachment of α-diimine nickel (II) catalysts on supports for ethylene polymerization with controlled morphology," *Catalysis Letters*, vol. 150, pp. 2322–2330, 2020.

[26] E. Kianfar, "Nanozeolites: synthesized, properties, applications," *Journal of Sol-Gel Science and Technology*, vol. 91, pp. 415–429, 2019.

[27] K. K. Pant and D. Kunzru, "Catalytic pyrolysis of N-heptane on unpromoted and potassium promoted calcium aluminates," *Chemical Engineering Journal*, vol. 87, pp. 219–225, 2002.

[28] J. Towfighi, H. Zimmermann, R. Karimzadeh, and M. Akbarnejad, "Steam cracking of naphtha in packed bed reactors," *Industrial & Engineering Chemistry Research*, vol. 41, pp. 1419–1424, 2002.

[29] F. C. Jentoft and B. C. Gates, "Solid-acid-Catalyzed alkane cracking mechanisms: evidence from reactions of small probe molecules," *Topics in Catalysis*, vol. 4, pp. 1–13, 1997.

[30] H. Liu and E. Kianfar, "Investigation the synthesis of nano-SAPO-34 catalyst prepared by different templates for MTO process," *Catalysis Letters*, vol. 151, 2020.

[31] E. Kianfar, M. Salimi, S. Hajimirzaee, and B. Koohestani, "Methanol to gasoline conversion over CuO/ZSM-5 catalyst synthesized using sonochemistry method," *International Journal of Chemical Reactor Engineering*, vol. 17, 2018.

[32] E. Kianfar, M. Salimi, V. Pirouzfar, and B. Koohestani, "Synthesis of modified catalyst and stabilization of CuO/NH4-ZSM-5 for conversion of methanol to gasoline," *International Journal of Applied Ceramic Technology*, vol. 15, pp. 734–741, 2018.

[33] E. Kianfar, M. Salimi, V. Pirouzfar, and B. Koohestani, "Synthesis and modification of zeolite ZSM-5 catalyst with solutions of calcium carbonate (CaCO3) and sodium carbonate (Na2CO3) for methanol to gasoline conversion," *International Journal of Chemical Reactor Engineering*, vol. 16, no. 7, Article ID 20170229, 2018.

[34] G. Bellussi and P. Pollesel, "Industrial applications of zeolite catalysts: production and uses of light olefins," *Studies in Surface Science and Catalysis*, vol. 158, pp. 1201–1212, 2005.

[35] M. A. den Hollander, M. Wissink, and M. Makkee, "Gasoline conversion: reactivity towards cracking with equilibrated FCC and ZSM-5 catalysts," *Applied Catalysis A: General*, vol. 223, pp. 85–102, 2002.

[36] J. S. Buchanan, "Reactions of model compounds over steamed ZSM-5 at simulated FCC reaction conditions," *Applied Catalysis A: General*, vol. 74, pp. 83–94, 1991.

[37] M. Kianfar, F. Kianfar, and E. Kianfar, "The effect of nanocomposites on the mechanic and morphological characteristics of NBR/PA6 blends," *American Journal of Oil and Chemical Technologies*, vol. 4, no. 1, pp. 29–44, 2016.

[38] F. Kianfar, S. R. M. Moghadam, and E. Kianfar, "Energy optimization of ilam gas refinery unit 100 by using HYSYS refinery software," *Indian Journal of Science and Technology*, vol. 8, no. S9, pp. 431–436, 2015.

[39] E. Kianfar, "Production and identification of vanadium oxide nanotubes," *Indian Journal of Science and Technology*, vol. 8, no. S9, pp. 455–464, 2015.

[40] F. Kianfar, S. R. M. Moghadam, and E. Kianfar, "Synthesis of spiro pyran by using silica-bonded N-propyldiethylenetriamine as recyclable basic catalyst," *Indian Journal of Science and Technology*, vol. 8, no. 11, Article ID 68669, 2015.

[41] E. Kianfar, "Recent advances in synthesis, properties, and applications of vanadium oxide nanotube," *Microchemical Journal*, vol. 145, pp. 966–978, 2019.

[42] S. Hajimirzaee, A. S. Mehr, and E. Kianfar, "Modified ZSM-5 zeolite for conversion of LPG to aromatics," *Polycyclic Aromatic Compounds*, 2020.

[43] E. Kianfar, "Investigation of the effect of crystallization temperature and time in synthesis of SAPO-34 catalyst for the production of light olefins," *Petroleum Chemistry*, vol. 61, pp. 527–537, 2021.

[44] X. Li, B. Shen, and C. Xu, "Interaction of titanium and iron oxide with ZSM-5 to tune the catalytic cracking of hydrocarbons," *Applied Catalysis A: General*, vol. 37, pp. 222–229, 2010.

[45] Y. Wei, F. Chang, Y. He et al., "Creating Mesopores in ZSM-5 for improving catalytic Cracking of hydrocarbons," *Surface Science and Catalysis*, vol. 165, pp. 539–542, 2007.

[46] X. Huang, Y. Zhu, and E. Kianfar, "Nano biosensors: properties, applications and electrochemical techniques," *Journal of Materials Research and Technology*, vol. 12, pp. 1649–1672, 2021.

[47] E. Kianfar, "Protein nanoparticles in drug delivery: animal protein, plant proteins and protein cages, albumin nanoparticles," *Journal of Nanobiotechnology*, vol. 19, p. 159, 2021.

[48] E. Kianfar, "Magnetic nanoparticles in targeted drug delivery: a review," *Journal of Superconductivity and Novel Magnetism*, vol. 34, 2021.

[49] R. Syah, M. Zahar, and E. Kianfar, "Nanoreactors: properties, applications and characterization," *International Journal of Chemical Reactor Engineering*, vol. 19, no. 10, pp. 981–1007, 2021.

[50] I. Raya, H. H. Kzar, Z. H. Mahmoud, A. Al A. Ahmed, A. Z. Ibatova, and E. Kianfar, "A review of gas sensors based on carbon nanomaterial," *Carbon Letters*, 2021.

[51] S. A. Jasim, M. M. Kadhim, V. Kn et al., "Molecular junctions: introduction and physical foundations, nanoelectrical conductivity and electronic structure and charge transfer in organic molecular junctions," *Brazilian Journal of Physics*, vol. 52, p. 31, 2022.

[52] A. Samimi, S. Zarinabadi, A. H. Shahbazi Kootenaei, A. Azimi, and M. Mirzaei, "Optimization of naphtha hydro-threating unit with continuous resuscitation due to the optimum temperature of octanizer unit reactors," *Advanced Journal of Chemistry-Section A*, vol. 3, no. Issue 2, pp. 165–180, 2020.

[53] A. Samimi, S. Zarinabadi, A. H. Shahbazi Kootenai, A. Azimi, and M. Mirzaei, "Optimization of the naphtha hydro treating unit (NHT) in order to increase feed in the refinery," *Eurasian Chemical Communications*, vol. 2, no. 1, pp. 150–161, 2020.

[54] L. Figueroa-Valverde, D. C. Francisco, R.-N. Marcela et al., "Design and synthesis of a diaza-bicyclo-naphthalen-oxiranyl-methanone derivative. Theoretical analysis of their interaction with cytochrome P450-17a1," *Chemical Methodologies*, vol. 3, no. 2, pp. 194–210, 2019.

[55] L. Wang, M. Xie, and L. Tao, "Conversion of light paraffins for preparing small olefins over ZSM-5 zeolites," *Catalysis Letters*, vol. 28, pp. 61–68, 1994.

[56] V. L. Zholobenko, L. M. Kustov, V. B. Kazansky, E. Loeffler, U. Lohse, and G. Oehlmann, "On the nature of the sites responsible for the enhancement of the cracking activity of HZSM-5 zeolites dealuminated under mild steaming conditions: Part 2," *Zeolites*, vol. 11, pp. 132–134, 1991.

[57] A. J. Maia, B. Louis, Y. L. Lam, and M. M. Pereira, "Ni-ZSM-5 catalysts: detailed characterization of metal sites for proper catalyst design," *Journal of Catalysis*, vol. 269, pp. 103–109, 2010.

[58] M. Rabiei, B. zeynizadeh, and M. Khanmirzaee, "The immobilized SbFx species on copper or nickel ferrite as magnetic nanocatalysts for fast and convenient reduction and reductive acetylation of nitroarenes as well Acetylation farylamines," *Journal of Applied Organometallic Chemistry*, vol. 1, no. 4, pp. 174–196, 2021.

[59] M. Bashirzadeh, "Green synthesis of quinoxaline derivatives at room temperature in ethylene glycol with h2so4/sio2 catalyst," *European Chemical Bulletin*, vol. 9, no. 1, pp. 33–37, 2020.

[60] V. Bakhtadze, V. Mosidze, T. Machaladze et al., "Activity of Pd-MnOx/CORDIERITE (Mg, Fe) 2Al4Si5O18) catalyst for carbon monoxide oxidation," *European Chemical Bulletin*, vol. 9, no. 2, pp. 75–77, 2020.

[61] S. B. Sapkal, S. Y. Guhe, S. N. Harke, B. R. Madje, and S. S. Gadekar, "Au-mops (3-morpholinopropane-1-sulfonic acid) coupled catalyst for the synthesis of 3-aminoalkylated indoles," *European Chemical Bulletin*, vol. 9, no. 3, pp. 82–86, 2020.

[62] V. G. Shtamburg, V. V. Shtamburg, A. A. Anishchenko, S. V. Shishkina, I. S. Konovalova, and A. V. Mazepa, "Interaction of ninhydrin with N-hydroxyurea and N-alkoxyureas in acetic acid," *European Chemical Bulletin*, vol. 9, no. 5, pp. 125–131, 2020.

[63] O. Mikhailov and D. Chachkov, "Novel oxidation degree–zn+ 3 in the macrocyclic compound with trans-di [benzo] porphyrazine and fluoride ligand: quantum-chemical consideration," *European Chemical Bulletin*, vol. 9, no. 7, pp. 160–163, 2020.

[64] A. M. Dar, N. A. Dangroo, S. Mir, and B. A. Dar, "The expeditious oxidation OF arylboronic acids to phenols By tertiary butyl hydroperoxide IN green aqueous ethanol," *European Chemical Bulletin*, vol. 9, no. 8, pp. 193–195, 2020.

[65] M. F. Gözükızıl, "pH effect on structural, morphological and optical properties of zno thin films produced by chemical bath deposition method," *European Chemical Bulletin*, vol. 9, no. 10, pp. 335–338, 2020.

[66] X. Wu, C. Li, Z. Zhou et al., "Circulating purification of cutting fluid: an overview," *International Journal of Advanced Manufacturing Technology*, vol. 117, pp. 2565–2600, 2021.

[67] X. Cui, C. Li, W. Ding et al., "Minimum quantity lubrication machining of aeronautical materials using carbon group nanolubricant: from mechanisms to application," *Chinese Journal of Aeronautics*, 2021.

[68] M. Wang, C. Jiang, S. Zhang, X. Song, Y. Tang, and H. Cheng, "Reversible calcium alloying enables a practical room-temperature rechargeable calcium-ion battery with a high discharge voltage," *Nature Chemistry*, vol. 10, no. 6, pp. 667–672, 2018.

[69] C. Xue, J. You, H. Zhang, S. Xiong, T. Yin, and Q. Huang, "Capacity of myofibrillar protein to adsorb characteristic fishy-odor compounds: effects of concentration, temperature, ionic strength, pH and yeast glucan addition," *Food Chemistry*, vol. 363, Article ID 130304, 2021.

[70] K. Zhang, L. Qiu, J. Tao et al., "Recovery of gallium from leach solutions of zinc refinery residues by stepwise solvent extraction with N235 and Cyanex 272," *Hydrometallurgy*, vol. 205, 2021.

[71] R. Wang, H. Xie, X. Lai, J. Liu, J. Li, and G. Qiu, "Visible light-enabled iron-catalyzed selenocyclization of N-methoxy-2-alkynylbenzamide," *Molecular Catalysis*, vol. 415, 2021.

[72] M. Yang, Q. Kong, W. Feng, W. Yao, and Q. Wang, "Hierarchical porous nitrogen, oxygen, and phosphorus ternary doped hollow biomass carbon spheres for high-speed and long-life potassium storage," *Carbon energy*, vol. 4, 2021.

[73] H. Wang, J. Cui, Y. Zhao, Z. Li, and J. Wang, "Highly efficient separation of 5-hydroxymethylfurfural from imidazolium-based ionic liquids," *Green Chemistry*, vol. 23, pp. 405–411, 2021.

[74] J. Wang, K. Ai, and L. Lu, "Flame-retardant porous hexagonal boron nitride for safe and effective radioactive iodine capture," *Journal of materials chemistry. A, Materials for energy and sustainability*, vol. 7, no. 28, Article ID 16858, 2019.

[75] J. Jia, Y. Cao, T. Wu et al., "Highly regio- and stereoselective markovnikov hydrosilylation of alkynes catalyzed by high-nuclearity {Co14} clusters," *ACS Catalysis*, vol. 11, no. 12, pp. 6944–6950, 2021.

[76] Y. Li, D. D. Macdonald, J. Yang, J. Qiu, and S. Wang, "Point defect model for the corrosion of steels in supercritical water: Part I, film growth kinetics," *Corrosion Science*, vol. 163, Article ID 108280, 2020.

[77] Y. Huang, C. An, Q. Zhang et al., "Cost-effective mechanochemical synthesis of highly dispersed supported transition metal catalysts for hydrogen storage," *Nano Energy*, vol. 80, Article ID 105535, 2021.

[78] K. Wakui, K. Sato, G. Sawada et al., "Cracking of n-butane over alkaline earth-containing HZSM-5 catalysts," *Catalysis Letters*, vol. 84, pp. 259–264, 2002.

[79] J. Lu, Z. Zhao, C. Xu, P. Zhang, and A. Duan, "FeHZSM-5 molecular sieves – highly active catalysts for catalytic cracking of isobutane to produce ethylene and propylene," *Catalysis Communications*, vol. 7, pp. 199–203, 2006.

[80] X. Wang, Z. Zhao, C. Xu, A. Duan, L. Zhang, and G. Jiang, "Effects of light rare earth on acidity and catalytic performance of HZSM-5 zeolite for catalytic cracking of butane to light olefin," *Journal of Rare Earths*, vol. 25, pp. 321–328, 2007.

[81] A. Keyvanloo, J. Towfighi, S. M. Sadrameli, and A. Mohamadalizadeh, "Investigating the effect of key factors, their interactions and optimization of naphtha steam cracking by statistical design of experiments," *Journal of Analytical and Applied Pyrolysis*, vol. 87, pp. 224–230, 2010.

[82] Y. Wei, Z. Liu, G. Wang et al., "Production of light olefins and aromatic hydrocarbons through catalytic cracking of naphtha at lowered temperature," *Studies in Surface Science and Catalysis*, vol. 158, pp. 1223–1230, 2005.

[83] K. Keyvanloo and J. Towfighi, "Comparing the catalytic performances of mixed molybdenum with cerium and lanthanide oxides supported on HZSM-5 by multiobjective optimization of catalyst compositions using nondominated sorting genetic algorithm," *Journal of Analytical and Applied Pyrolysis*, vol. 88, pp. 140–148, 2010.

[84] F. Khodadadian, ""Stability Enhancment of zeolite Catalysts in Thermal catalytic Cracking of Naphtha by rare earth elements", thesis submitted in partial fulfillment of the

requirements for the degree of master of science (M.Sc.)," in *Chemical Engineering*Tarbiat Modares University, Iran, 2011.

[85] M. Abraha, X. Wu, and R. G. Anthony, "Effects of particle size and modified SAPO-34 on conversion of methanol to light olefins and dimethyl ether," *Surface Science and Catalysis*, vol. 133, pp. 211–218, 2001.

[86] M. Salmasi, Sh. Fatemi, and A. Taheri, "Improvement of light olefins selectivity and catalyst lifetime in MTO reaction; using Ni and Mg-modified SAPO-34 synthesized by combination of two templates," *Journal of Industrial and Engineering Chemistry*, vol. 17, pp. 755–761, 2011.

[87] X. Wu, M. G. Abraha, and R. G. Anthony, "Methanol conversion on SAPO-34: reaction condition for fixed-bed reactor," *Applied Catalysis A: General*, vol. 260, pp. 63–69, 2004.

[88] G. Zhao, J. Teng, Z. Xie, W. Yang, Q. Chen, and Y. Tang, "Catalytic cracking reactions of C4-olefin over zeolites H -ZSM-5, H-mordenite and H-SAPO-34," *Surface Science and Catalysis*, vol. 170, pp. 1307–1312, 2007.

[89] X. Zhu, S. Liu, Y. Song, and L. Xu, "Catalytic cracking of C4 alkenes to propene and ethene: influences of zeolites pore structures and Si/Al_2 ratios," *Applied Catalysis A: General*, vol. 288, pp. 134–142, 2005.

[90] N. taghipur, "Synthesis of metals nano scale over zeolites for produce light olefins," in *Chemical Engineering*Thesis Submitted in Partial Fulfillment of the Requirements for the Degree of Master of Science (M.Sc.), Tarbiat Modares University, Iran, 2012.

[91] J. B. Casady and R. W. Johnson, "Status of silicon carbide (SiC) as a wide-bandgap semiconductor for high-temperature applications: a review," *Solid-State Electronics*, vol. 39, pp. 1409–1422, 1996.

[92] J. A. Cornell, *How to Apply Response Surface Methodology*, American Society for Quality Control, Wi, USA, 1990.

[93] Y. Hang, M. Qu, and S. Ukkusuri, "Optimizing the design of a solar cooling system using central composite design techniques," *Energy and Buildings*, vol. 43, pp. 988–994, 2011.

[94] J. Bi, M. Liu, Ch. Song, X. Wang, and X. Guo, "C2 –C4 light olefins from bioethanol catalyzed by Ce-modified nanocrystalline HZSM-5 zeolite catalysts," *Applied Catalysis B: Environmental*, vol. 107, pp. 68–76, 2011.

[95] I. Barros, V. S. Braga, S. Pinto et al., "Effects of niobium addition on ZSM-5 studied by thermal and spectroscopy methods," *Microporous and Mesoporous Materials*, vol. 109, pp. 485–493, 2008.

[96] J. A. Botas, D. P. Serrano, A. García, J. De Vicente, and R. Ramos a, "Catalytic conversion of rapeseed oil into raw chemicals and fuels over Ni- and Mo-modified nanocrystalline ZSM-5 zeolite," *Catalysis Today*, vol. 195, pp. 59–70, 2012.

[97] J. Tan, Z. Liu, X. Bao, X. Liu, and X. Han, "Crystallization and Si incorporation mechanisms of SAPO-34," *Microporous and Mesoporous Materials*, vol. 53, pp. 97–108, 2002.

[98] E. Kianfar, M. Baghernejad, and Y. Rahimdashti, "Study synthesis of vanadium oxide nanotubes with two template hexadecylamin and hexylamine," *Biological Forum*, vol. 7, pp. 1671–1685, 2015.

[99] E. kianfar, *Synthesizing of Vanadium Oxide Nanotubes Using Hydrothermal and Ultrasonic Method*, pp. 1–80, Lambert Academic Publishing, CA, USA, 2020.

[100] E. Kianfar, V. Pirouzfar, and H. Sakhaeinia, "An experimental study on absorption/stripping CO2 using Monoethanol amine hollow fiber membrane contactor," *Journal of Taiwan Institution of Chemical Engineers*, vol. 80, pp. 954–962, 2017.

[101] E. Kianfar and C. Viet, "Polymeric membranes on base of PolyMethyl methacrylate for air separation: a review," *Journal of Materials Research and Technology*, vol. 10, pp. 1437–1461, 2021.

[102] S. nmousavian, P. Faravar, Z. Zarei, R. zimikia, M. G. Monjezi, and E. kianfar, "Modeling and simulation absorption of CO2 using hollow fiber membranes (HFM) with mono-ethanol amine with computational fluid dynamics," *Journal of Environmental Chemical Engineering*, vol. 8, no. 4, Article ID 103946, 2020.

[103] Y. Sugi, Y. Kubota, K. Komura et al., "Shape-selective alkylation and related reactions of mononuclear aromatic hydrocarbons over H-ZSM-5 zeolites modified with lanthanum and cerium oxides," *Applied Catalysis A: General*, vol. 299, pp. 157–166, 2006.

[104] P. Me riaudeau, V. A. Tuan, L. N. Hung, F. Lefebvre, and H. P. Nguyen, "Zirconium-SAPO-11: the peculiar effect of zirconium addition on the catalytic properties for n-butene isomerization," *Journal of the Chemical Society, Faraday Transactions*, vol. 93, pp. 4201–4206, 1997.

[105] G. Elordi, M. Olazar, M. Artetxe, P. Castaño, and J. Bilbao, "Effect of the acidity of the HZSM-5 zeolite catalyst on the cracking of high density polyethylene in a conical spouted bed reactor," *Applied Catalysis A: General*, vol. 415, pp. 89–95, 2012.

[106] Z. Yang, L. Zhang, Y. Zhou, and H. Wang, "Lichen Wen, and Ehsan Kianfar, Investigation of effective parameters on SAPO-34 Nano catalyst the methanol-to-olefin conversion process: a review," *Reviews in Inorganic Chemistry*, vol. 40, no. 3, pp. 91–105, 2020.

[107] C. Gao, J. Liao, J. Lu, J. Ma, and E. Kianfar, "The effect of nanoparticles on gas permeability with polyimide membranes and network hybrid membranes: a review," *Reviews in Inorganic Chemistry*, vol. 41, pp. 1–20, 2020.

[108] E. Kianfar, M. Salimi, and B. Koohestani, *Zeolite CATALYST: A Review on the Production of Light Olefins*, pp. 1–116, Publisher: Lambert Academic Publishing, CA, USA, 2020.

[109] E. Kianfar, *Investigation on Catalysts of "Methanol to Light Olefins"*, pp. 1–168, Lambert Academic Publishing, CA, USA, 2020.

[110] E. Kianfar, "Application of nanotechnology in enhanced recovery oil and gas," *Importance & Applications of Nanotechnology*, vol. 5, pp. 16–21, MedDocs Publishers, NV, USA, 2020.

[111] E. Kianfar, "Catalytic properties of nanomaterials and factors affecting it," *Importance & Applications of Nanotechnology*, vol. 5, pp. 22–25, MedDocs Publishers, NV, USA, 2020.

[112] E. Kianfar, "Introducing the application of nanotechnology in lithium-ion battery," *Importance & Applications of Nanotechnology*, vol. 4, pp. 1–7, MedDocs Publishers, NV, USA, 2020.

[113] E. Kianfar and H. Mazaheri, "Synthesis of nanocomposite (CAU-10-H) thin-film nanocomposite (TFN) membrane for removal of color from the water," *Fine Chemical Engineering*, vol. 1, pp. 83–91, 2020.

[114] E. Kianfar, M. Salimi, and B. Koohestani, "Methanol to gasoline conversion over CuO/ZSM-5 catalyst synthesized and influence of water on conversion," *Fine Chemical Engineering*, vol. 1, pp. 75–82, 2020.

[115] E. Kianfar, "An experimental study PVDF and PSF hollow fiber membranes for chemical absorption carbon dioxide," *Fine Chemical Engineering*, vol. 1, pp. 92–103, 2020.

[116] E. Kianfar and S. Mafi, "Ionic liquids: properties, application, and synthesis," *Fine Chemical Engineering*, vol. 2, pp. 22–31, 2020.

[117] S. M. Faghih and E. Kianfar, "Modeling of fluid bed reactor of ethylene dichloride production in Abadan Petrochemical based on three-phase hydrodynamic model," *International Journal of Chemical Reactor Engineering*, vol. 16, pp. 1–14, 2018.

[118] E. Kianfar and H. Mazaheri, "Methanol to gasoline: a sustainable transport fuel," in *Book: Advances in Chemistry Research*, J. C. taylor, Ed., Vol. 66, Nova Science Publishers, Inc., NY, USA, 2020.

[119] A. Kianfar, "Comparison and assessment on performance of zeolite catalyst based selective for theProcess methanol to gasoline: a review," in *Advances in Chemistry Research*Vol. 63, Nova Science Publishers, Inc., NewYork, USA, 2020.

[120] E. Kianfar, M. Salimi, and F. Kianfar, "CO2/N2 separation using polyvinyl chloride iso-phthalic acid/aluminium nitrate nanocomposite membrane," *Macromolecular Research*, vol. 27, pp. 83–89, 2019.

[121] E. Kianfar, "Synthesis of characterization Nanoparticles isophthalic acid/aluminum nitrate (CAU-10-H) using method hydrothermal," *Advances in Chemistry Research*, Nova Science Publishers, Inc., NY, USA, 2020.

[122] E. Kianfar, "CO2 capture with ionic liquids: a review," *Advances in Chemistry Research*, Vol. 67, Nova Science Publishers, Inc., , NY, USA, 2020.

[123] E. Kianfar, "Enhanced light olefins production via methanol dehydration over promoted SAPO-34," *Advances in Chemistry Research*, Chapter: 4, vol. 63, Nova Science Publishers, Inc., NY, USA, 2020.

[124] E. Kianfar, "Gas hydrate: applications, structure, formation, separation processes, Thermodynamics," in *Advances in Chemistry Research*, J. C. Taylor, Ed., Vol. 62, Nova Science Publishers, Inc., NY, USA, 2020.

[125] M. Alyani, A. Mohamadalizadehb, J. Towfighi, and N. Hosseini, "Thermal catalytic cracking of naphtha over multi wall carbon nanotube catalysts," *Journal of Analytical and Applied Pyrolysis*, vol. 98, pp. 7–14, 2012.